ARTICLES
https://doi.org/10.1038/s41556-018-0141-0

nature cell biology

Corrected: Publisher Correction

IRE1α governs cytoskeleton remodelling and cell migration through a direct interaction with filamin A

Hery Urra[1,2,3], Daniel R. Henriquez[2,4], José Cánovas[1], David Villarroel-Campos[2,4], Amado Carreras-Sureda[1,2,3], Eduardo Pulgar[1,5], Emiliano Molina[4,6], Younis M. Hazari[1,2,3], Celia M. Limia[1,2,3], Sebastián Alvarez-Rojas[2,4], Ricardo Figueroa[1,3], Rene L. Vidal[1,2,7], Diego A. Rodriguez[3], Claudia A. Rivera[1,2,7], Felipe A. Court[2,7], Andrés Couve[1,8], Ling Qi[9], Eric Chevet[10,11], Ryoko Akai[12], Takao Iwawaki[12], Miguel L. Concha[1,2,5], Álvaro Glavic[4,6], Christian Gonzalez-Billault[2,4] and Claudio Hetz[1,2,3,13,14]*

Maintenance of endoplasmic reticulum (ER) proteostasis is controlled by a signalling network known as the unfolded protein response (UPR). Here, we identified filamin A as a major binding partner of the ER stress transducer IRE1α. Filamin A is an actin crosslinking factor involved in cytoskeleton remodelling. We show that IRE1α controls actin cytoskeleton dynamics and affects cell migration upstream of filamin A. The regulation of cytoskeleton dynamics by IRE1α is independent of its canonical role as a UPR mediator, serving instead as a scaffold that recruits and regulates filamin A. Targeting IRE1α expression in mice affected normal brain development, generating a phenotype resembling periventricular heterotopia, a disease linked to the loss of function of filamin A. IRE1α also modulated cell movement and cytoskeleton dynamics in fly and zebrafish models. This study unveils an unanticipated biological function of IRE1α in cell migration, whereby filamin A operates as an interphase between the UPR and the actin cytoskeleton.

The ER is the largest intracellular organelle and is involved in protein synthesis, folding and secretion. A series of physiological and pathological conditions favour the accumulation of misfolded proteins at the ER lumen, resulting in a cellular state known as ER stress[1]. To cope with misfolded proteins, cells engage a dynamic signalling pathway known as the UPR[2]. In vertebrates, the UPR has evolved towards the establishment of a network of interconnected signalling cascades initiated by three types of transducers known as inositol-requiring enzyme 1 (IRE1) alpha and beta, activating transcription factor-6 (ATF6) alpha and beta, and protein kinase RNA (PKR)-like ER kinase (PERK). The UPR controls specific transcription factors that feedback to restore proteostasis[1] or activate apoptotic programmes[3]. ER stress is also emerging as a relevant factor driving diverse pathological conditions, including cancer, diabetes, inflammatory diseases and neurodegeneration[4,5].

IRE1α is a serine/threonine protein kinase and endoribonuclease that catalyses the unconventional processing of the messenger RNA encoding X-box binding protein 1 (XBP1), resulting in the expression of an active transcription factor (XBP1s) that enforces adaptation programmes[6,7]. In addition to the classical role of IRE1α as an ER stress mediator, a series of novel physiological outputs of the pathway have been reported that are dependent on XBP1s and affect cell differentiation, angiogenesis and energy metabolism[2]. IRE1α signalling is tightly regulated by the assembly of protein complexes that fine-tune its activity, a platform referred to as the UPRosome[8]. Thus, defining the IRE1α interactome may reveal unexpected functions to delineate the significance of the UPR in cell physiology.

Here, we performed a protein–protein interaction screen and identified filamin A as a major IRE1α binding partner. Filamin A is involved in crosslinking polymerized actin and has a crucial role in adhesion, cell morphology and migration[9]. We demonstrate that the IRE1α–filamin A axis regulates actin cytoskeleton dynamics and cell movement. Unexpectedly, this function of IRE1α is controlled by its dimerization, independent of its canonical signalling as a UPR mediator. We also provide evidence indicating that the regulation of cell migration by IRE1α is disease relevant and evolutionarily conserved. Overall, our results reveal an unanticipated site of control of actin cytoskeleton dynamics from the ER, where IRE1α serves as a scaffold to engage filamin A signalling and modulate cell movement.

[1]Biomedical Neuroscience Institute, Faculty of Medicine, University of Chile, Santiago, Chile. [2]Center for Geroscience, Brain Health and Metabolism (GERO), Santiago, Chile. [3]Program of Cellular and Molecular Biology, Institute of Biomedical Sciences, University of Chile, Santiago, Chile. [4]Department of Biology, Faculty of Sciences, University of Chile, Santiago, Chile. [5]Program of Anatomy and Developmental Biology, Institute of Biomedical Sciences, University of Chile, Santiago, Chile. [6]Center for Genome Regulation, Faculty of Sciences, University of Chile, Santiago, Chile. [7]Center for Integrative Biology, Faculty of Sciences, Universidad Mayor, Santiago, Chile. [8]Department of Neuroscience, Faculty of Medicine, University of Chile, Santiago, Chile. [9]Department of Molecular and Integrative Physiology, Division of Metabolism, Endocrinology and Diabetes, The University of Michigan Medical School, Ann Arbor, MI, USA. [10]INSERM U1242 Chemistry, Oncogenesis, Stress and Signaling, University of Rennes 1, Rennes, France. [11]Centre de Lutte contre le Cancer Eugène Marquis, Rennes, France. [12]Division of Cell Medicine, Department of Life Science, Medical Research Institute, Kanazawa Medical University, Uchinada, Japan. [13]The Buck Institute for Research in Aging, Novato, CA, USA. [14]Department of Immunology and Infectious Diseases, Harvard School of Public Health, Boston, MA, USA. *e-mail: chetz@med.uchile.cl

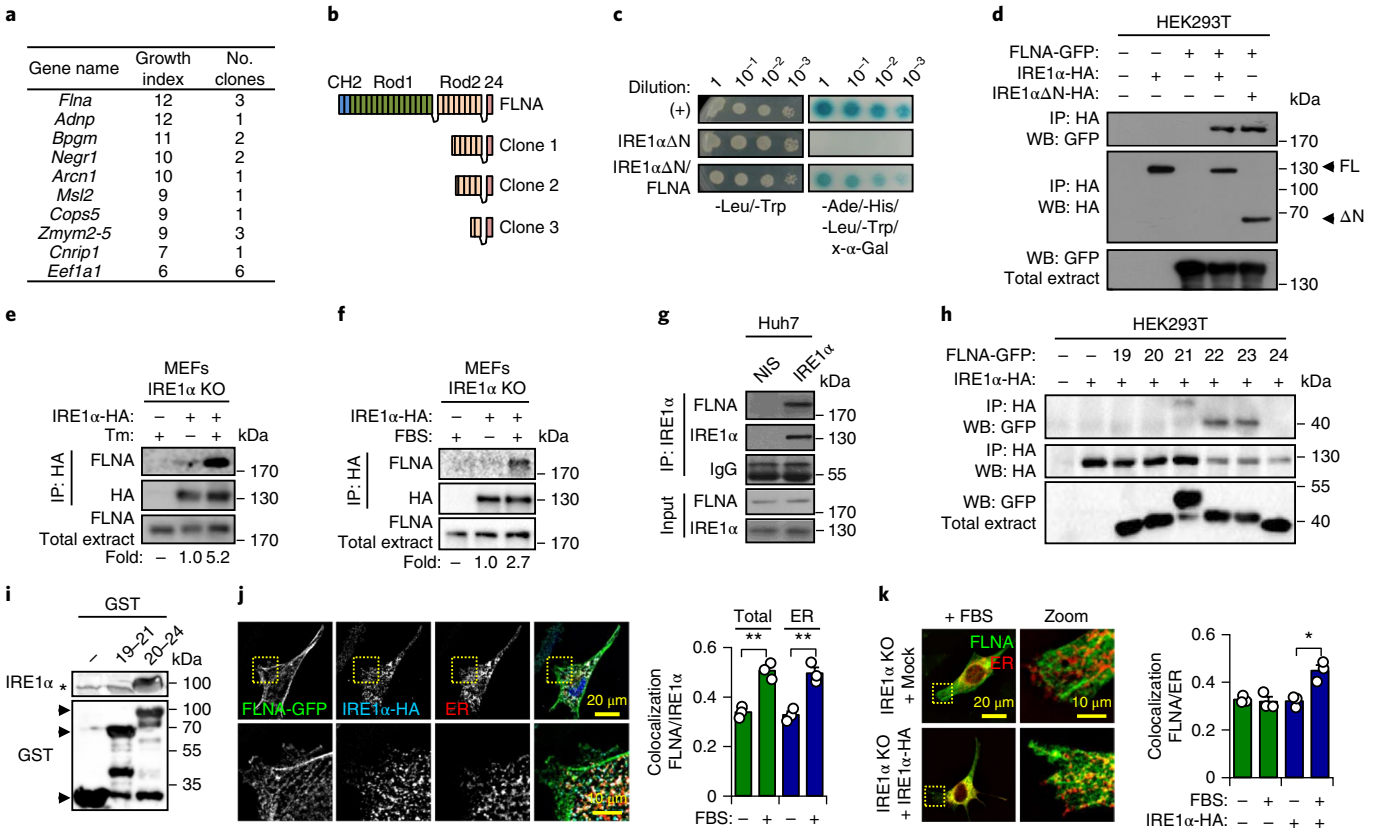

Fig. 1 | IRE1α physically interacts with filamin A. a, Results of the yeast two-hybrid screen of the cytosolic domain of IRE1α and the Matchmaker pretransformed cDNA library from adult mouse brain. The yeast growth index and the number of clones obtained are indicated. **b**, Representation of the primary structure of filamin A (FLNA) and the clones obtained in **a**. The CH2, Rod1, Rod2 and the IgG 24 domains are shown. **c**, Validation of the yeast two-hybrid assay using IRE1α-ΔN and wild-type filamin A. (+), positive control for the assay. Data show one out of three experiments, with similar results obtained. **d**, Co-immunoprecipitation (IP) of HA-tagged IRE1α full lenght (FL) or the cytosolic portion of IRE1α (ΔN) and GFP-tagged filamin A was assessed by western blotting (WB) using HEK293T cells. **e**, Co-immunoprecipitation of HA-tagged IRE1α and endogenous filamin A in IRE1α knockout (KO) MEFs reconstituted with an IRE1α-HA expression vector in cells treated with 500 ng ml^{-1} of tunicamycin (Tm) for 2 h. **f**, Co-immunoprecipitation of starved cells described in **e** treated with 3% FBS for 30 min. **g**, Co-immunoprecipitation of endogenous filamin A and IRE1α in Huh7 cells. A non-immune serum (NIS) was used as a control. **h**, Co-immunoprecipitation of HA-tagged IRE1α and individual domains of GFP-tagged filamin A spanning IgG repeats from 19 to 24 in HEK293T cells. **i**, In vitro pull-down of recombinant GST-fused domains of filamin A (19-21 and 21-24) and recombinant cytosolic IRE1α portion (IRE1α-ΔN) (asterisk indicates nonspecific band). **j**, Left, immunofluorescence images of MEFs expressing filamin A-GFP, IRE1α-HA and KDEL-RFP stimulated with 3% FBS for 30 min. Right, colocalization results of IRE1α-HA and filamin A-GFP restricted to the ER or total area ($n = 3$ independent experiments, 50 cells in total). **k**, Left, confocal images of CRISPR–Cas9 IRE1α KO cells or reconstituted with IRE1α-HA expressing filamin A-GFP and KDEL-RFP, stimulated with 3% FBS for 60 min. Right, colocalization results of filamin A-GFP and KDEL-RFP ($n = 3$ independent experiments, 50 cells in total). In panels **j** and **k** the area with higher magnification is shown (yellow squares). In all panels, data are shown as the mean ± s.e.m.; one-way ANOVA followed by Tukey's test. *$P < 0.05$ and **$P < 0.01$. Blots represent one out of two (**f**), three (**d**,**e**,**g**,**i**) or four (**h**) experiments, with similar results obtained.

Results

Direct interaction between filamin A and IRE1α. To identify new IRE1α-interacting proteins we performed a yeast two-hybrid screen using the Matchmaker pretransformed complementary DNA library together with the cytosolic domain of IRE1α (IRE1α-ΔN) as bait. Multiple candidates were found (Supplementary Table 1) to be involved in different biological processes (Supplementary Fig. 1A,B), including COPS5, a known IRE1α binding partner[10]. Among the top ten candidates selected on the basis of the growth index, filamin A presented the strongest interaction (Fig. 1a). Filamin A is an actin-binding protein involved in the orthogonal crosslinking of polymerized actin[9]. It is composed of 24 IgG-like repeats, containing several domains including the CH2 domain, Rod1 and Rod2, and an IgG-like 24 repeat involved in filamin A dimerization[11]. All clones selected corresponded to the carboxy-terminal portion of filamin A (Fig. 1b,c).

To validate our findings, we transfected HEK293T cells with expression vectors for full-length HA (human influenza hemagglutinin)-tagged IRE1α (IRE1α-HA) and a filamin A construct fused to green fluorescent protein (GFP) at the C-terminal region (filamin A-GFP). Immunoprecipitation of IRE1α-HA revealed a clear association of filamin A with the cytosolic domain of IRE1α (Fig. 1d). Additionally, we detected an association between IRE1α-HA and endogenous filamin A in IRE1α knockout mouse embryonic fibroblasts (MEFs) reconstituted with physiological levels of IRE1α[12] (Fig. 1e; see controls in Supplementary Fig. 1C). Interestingly, this interaction was enhanced under ER stress induced by tunicamycin, a pharmacological inhibitor of N-linked glycosylation (Fig. 1e), or with fetal bovine serum (FBS), a pro-migratory stimulus (Fig. 1f). We also corroborated the existence of an endogenous protein complex in Huh7 cells (Fig. 1g). Using individual IgG-like repeats of filamin A, we demonstrated that domains 22–23

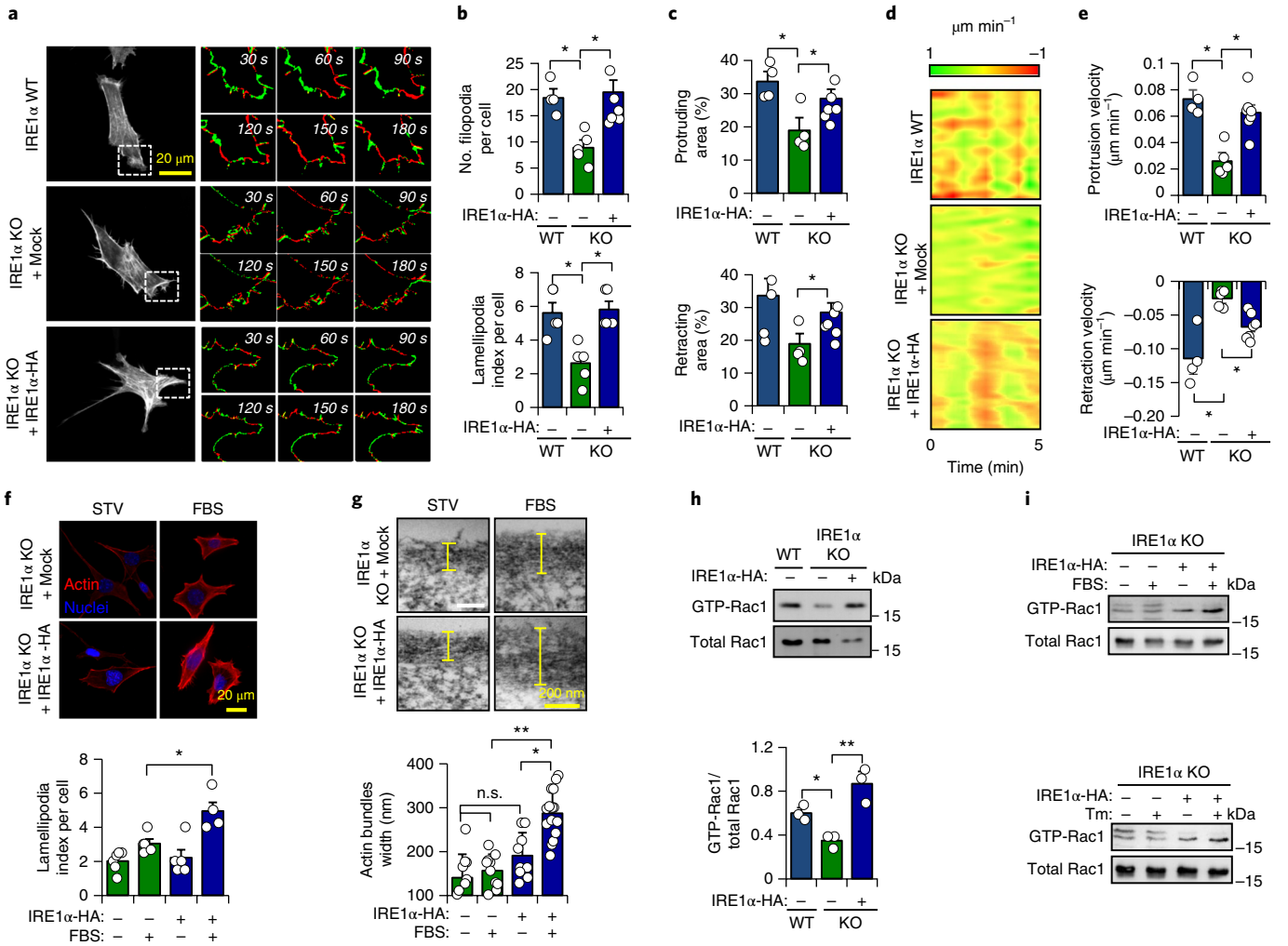

Fig. 2 | IRE1α regulates actin cytoskeleton dynamics and Rac1 activation. a, WT, IRE1α KO or IRE1α-HA-reconstituted cells were transfected with LifeAct and time-lapse confocal microscopy recordings were made every 30 s for 5 min. Segmentation was used to obtain protruding area (green) and retracting areas (red). Regions in dotted white squares are magnified in time-lapse images on the right. **b**, Top, the number of filopodia per cell was determined using ADAPT software. Bottom, the number of octants showing lamellipodia was evaluated per cell. **c**, The average signal over time of the protruding cell area or the retracting cell area was quantified from experiments presented in **a**. **d**, Heatmaps of LifeAct signal distribution along the cell determined by ADAPT software. **e**, The velocity of protrusions and retractions. For **b–e**, $n=5$, $n=5$ and $n=7$ independent experiments were determined for WT, IRE1α KO and IRE1α-HA, respectively. **f**, Top, IRE1α KO and IRE1α-HA-reconstituted cells were starved (STV) and then stimulated with 3% FBS for 30 min and stained with phalloidin-coupled to rodamine. Bottom, quantification of lamellipodia index per cell as described in **b** ($n=3$ independent experiments). **g**, Top, electron microscopy sections of cortical actin (bundles) in IRE1α KO and IRE1α-HA-reconstituted cells treated with 3% FBS for 30 min (×67,000 magnification). Bottom, quantification of width (yellow bars above) of actin bundles ($n=3$, 10 cells in total). **h**, Top, pull-down assay using GST-CRIB domain followed by western blot analysis to evaluate Rac1 activation of WT, IRE1α KO and IRE1α-HA-reconstituted cells. Bottom, Rac1-GTP levels were quantified and normalized to total Rac1 ($n=4$ independent experiments). **i**, IRE1α KO and IRE1α-HA-reconstituted cells were treated with 3% FBS for 1 h (top) or 100 ng ml^{-1} of Tm for 2 h (bottom). Rac1-GTP levels were evaluated by a pull-down assay using GST-CRIB domain followed by western blot analysis (data represent one out of three experiments, with similar results obtained). In all panels, data are shown as the mean ± s.e.m.; one-way ANOVA followed by Tukey's test. n.s., not significant, $^{*}P<0.05$ and $^{**}P<0.01$.

account for the interaction with IRE1α (Fig. 1h). These domains are central to the interaction with several signalling proteins, but they are unrelated to its ability to associate with polymerized actin[9]. Finally, using recombinant proteins, we replicated the direct binding of IRE1α to a fragment of filamin A spanning the 20–24 IgG-like repeat region, but not to the adjacent domain (Fig. 1i).

Quantification of colocalization using the Manders coefficient between IRE1α-HA and filamin A-GFP showed an enhanced association after stimulation of cells with FBS. Similar results were obtained when the analysis was confined to the ER (KDEL-RFP signal) (Fig. 1j), suggesting that filamin A relocates to the ER in close proximity to IRE1α. Importantly, the redistribution of filamin A to the ER was dependent on the expression of IRE1α (Fig. 1k). Taken together, these results indicate that filamin A interacts directly with IRE1α at the ER in multiple cellular systems.

IRE1α controls the dynamics of the actin cytoskeleton. Since filamin A has an active role in modulating morphological changes through local actin cytoskeleton remodelling[13], we tested the contribution of IRE1α to this process. We monitored actin cytoskeleton dynamics using LifeAct[14]. Time-lapse confocal microscopy of IRE1α-deficient cells revealed a reduced number of filopodia and lamellipodial protrusions (lamellipodia index) per cell (Fig. 2a,b; Supplementary Movie 1). In addition, the temporal dynamics

of cortical filamentous actin (F-actin), measured by the total area showing protrusions and retractions over time, presented a marked decrease in IRE1α-deficient cells (Fig. 2a-c; Supplementary Fig. 2A). This observation correlated with an altered distribution of polymerized actin across the cell upon targeting IRE1α expression (Fig. 2d; Supplementary Fig. 2B). Furthermore, the velocity of protrusions and retractions was dramatically reduced in IRE1α-null cells (Fig. 2e). For comparison, we also analysed filamin A-deficient cells (Supplementary Fig. 2C). Similar results were obtained when the lamellipodia index was evaluated in fixed cells (Fig. 2f). In addition, electron microscopy analysis of the distribution of cortical actin bundles, a structure highly concentrated in crosslinked actin[13], indicated a narrower area of actin bundles in IRE1α-deficient cells (Fig. 2g).

Actin cytoskeleton dynamics is dependent on the activity of small GTPases from the RhoA family[15]. Therefore, we evaluated the activity of Rac1, a RhoA GTPase that mediates the formation of actin protrusions in different cells types[15] and is regulated by filamin A[16]. The amount of active Rac1 coupled to GTP was decreased in IRE1α-null cells as determined using pull-down assays with the recombinant CRIB1 domain (amino acids 67–150) of p21-activated kinase (PAK1) as bait (Fig. 2h). Remarkably, stimulation with FBS or ER stress enhanced the activation of Rac1 in an IRE1α-dependent manner (Fig. 2i). These results indicate that IRE1α expression modulates actin cytoskeleton dynamics and Rac1 activation.

IRE1α deficiency impairs cell migration. We then determined whether IRE1α regulates cell movement as a readout of cytoskeleton alterations. Stimulation of IRE1α knockout cells with FBS revealed a significant decrease in cell migration in wound-healing assays compared to control cells (Fig. 3a). Similar results were obtained when transmigration was evaluated using the Boyden chamber assay (Fig. 3b). As a control, we measured cell proliferation, a parameter that was not modified in IRE1α-null cells (Supplementary Fig. 3A). Importantly, filamin A (*Flna*) knockout MEFs presented a similar extent of cell movement impairment as IRE1α-deficient cells (Fig. 3b; Supplementary Fig. 3B). Targeting IRE1α expression using short hairpin RNAs (shRNAs) or via clustered regularly interspaced short palindromic repeats (CRISPR)–Cas9 also led to a significant attenuation of cell migration in MEFs (Fig. 3c,d). Notably, targeting IRE1α expression affected cell movement in different cell lines (Fig. 3e; Supplementary Figs. 3C, and 8A). Finally, transient overexpression of IRE1α-HA in wild-type MEFs also enhanced cell migration (Supplementary Fig. 3D).

We next investigated whether filamin A is involved in the regulation of cell movement by IRE1α. Remarkably, the impairment of cell movement generated by knocking down IRE1α was reversed by the overexpression of filamin A (Fig. 3f; Supplementary Fig. 3E). In sharp contrast, overexpression of IRE1α failed to enhance cell migration in filamin A-null cells (Fig. 3g; Supplementary Fig. 3F). Thus, IRE1α requires filamin A to regulate cell migration. In addition, as reported in filamin A-null cells[17,18], IRE1α deficiency led to decreased ER and cell spreading upon attachment (Fig. 3h) and reduced cell adhesion (Fig. 3i).

Recently, it was described that PERK interacts with filamin A, affecting actin localization and the formation of ER–plasma membrane contact sites[19]. Thus, we determined the contribution of other UPR signalling branches to cell movement. Knocking down PERK or inhibiting it with GSK2606414 reduced cell migration with a similar ratio in both IRE1α-null and control cells (Supplementary Fig. 3G,H). This result suggests that the effects of IRE1α in cell migration are independent of PERK signalling. In contrast, knocking down ATF6 did not affect cell migration in MEFs (Supplementary Fig. 3I).

IRE1α regulates cell migration by interacting with filamin A. An analysis of the primary sequence of IRE1α indicated the presence of a proline-rich domain at the distal C-terminal region that is similar to a SH3-binding domain (XXPXXP or PXXPX) but of unknown function and structure[20] (Fig. 4a). Although filamin A does not contain an SH3 domain, it associates with several proteins containing proline-rich sequences[11]. We performed a pull-down assay using a region containing the proline-rich portion of IRE1α (previously named F11[21]) and observed a positive interaction with endogenous filamin A (Fig. 4b) but not with a different IRE1α region (F6 peptide; Fig. 4c). We repeated the pull-down assay and then performed Coomassie Blue staining and a mass spectrometry analysis to identify the most abundant proteins. Remarkably, filamin A was one of the major F11-binding partners found in this screen (Fig. 4d).

We then tested the contribution of the proline-rich domain of IRE1α to cell movement. Deletion of the complete F11 sequence abrogated the ability of IRE1α to enhance cell migration (Fig. 4e). Mutagenesis of the proline-rich domain by deleting the fragment spanning amino acids 965–977 of IRE1α (IRE1αΔ^{965}) or by replacing all three proline residues to alanine (IRE1α^{AAAA}) (Fig. 4a) did not affect the RNase activity of IRE1α (Fig. 4f, bottom panel), but fully blocked the ability of IRE1α to regulate cell migration (Fig. 4g) and actin cytoskeleton remodelling (Fig. 4h; Supplementary Fig. 4). These experiments fully dissected the activity of IRE1α on UPR and cell migration. In agreement with these findings, a reduction in the binding between IRE1α and filamin A was observed when IRE1αΔ^{965} and IRE1α^{AAAA} mutants were tested (Fig. 4i). We also performed competition experiments using different F11 peptide mutants. The expression of the F11 peptide disrupted the interaction between the filamin A-22 domain and IRE1α-HA in co-immunoprecipitation experiments, whereas this effect was attenuated by mutations in the proline-rich region (Fig. 4j,k). Overall, our results suggest that the physical interaction between filamin A and IRE1α is required to enhance cell migration.

IRE1α is an upstream regulator of filamin A phosphorylation. The activity of filamin A in cytoskeleton dynamics and cell migration depends on the phosphorylation of serine 2,152 (S2152)[11,22]. A robust enhancement of filamin A phosphorylation was detected in cells stimulated with serum in IRE1α-expressing MEFs compared with knockout cells (Fig. 5a,b). Similarly, stimulation of cells with tunicamycin showed significantly higher filamin A phosphorylation in IRE1α-expressing cells (Fig. 5a,c). The remaining phosphorylation observed in IRE1α-deficient cells was independent of PERK, as demonstrated by transfecting cells with small interfering (siRNAs) or by treating cells with GSK2606414 (Supplementary Fig. 5A). We also determined that the fraction of filamin A bound to IRE1α is phosphorylated in cells stimulated with FBS (Fig. 5d) or tunicamycin (Fig. 5e).

We then determined whether filamin A phosphorylation is required for the modulation of actin cytoskeleton dynamics downstream of IRE1α. Transient transfection of wild-type filamin A, and not a S2152A mutant, restored the normal levels of actin cytoskeleton dynamics and cell migration observed when IRE1α was targeted (Fig. 5f,g; Supplementary Fig. 5B–E). In addition, simple overexpression of filamin A resulted in its phosphorylation (Supplementary Fig. 5F), which may explain the ability of this strategy to bypass IRE1α deficiency. Importantly, deletion of the filamin A-binding domain in IRE1α led to in reduced filamin A phosphorylation (Fig. 5h).

Based on our results, we hypothesized that IRE1α serves as a scaffold to recruit the kinases involved in filamin A phosphorylation. The most relevant regulators of filamin A are PAK1[16], CDK4[23], PKCα[24] and MEKK4[22,25]. A pharmacological screen indicated that PAK1 and PKCα mediated filamin A phosphorylation (Supplementary Fig. 5G). These results were then validated using siRNAs. Knocking down PKCα reduced filamin A phosphorylation under ER stress (Fig. 5i; Supplementary Fig. 5H) and FBS stimulation (Supplementary Fig. 5I). In addition, IRE1α deficiency

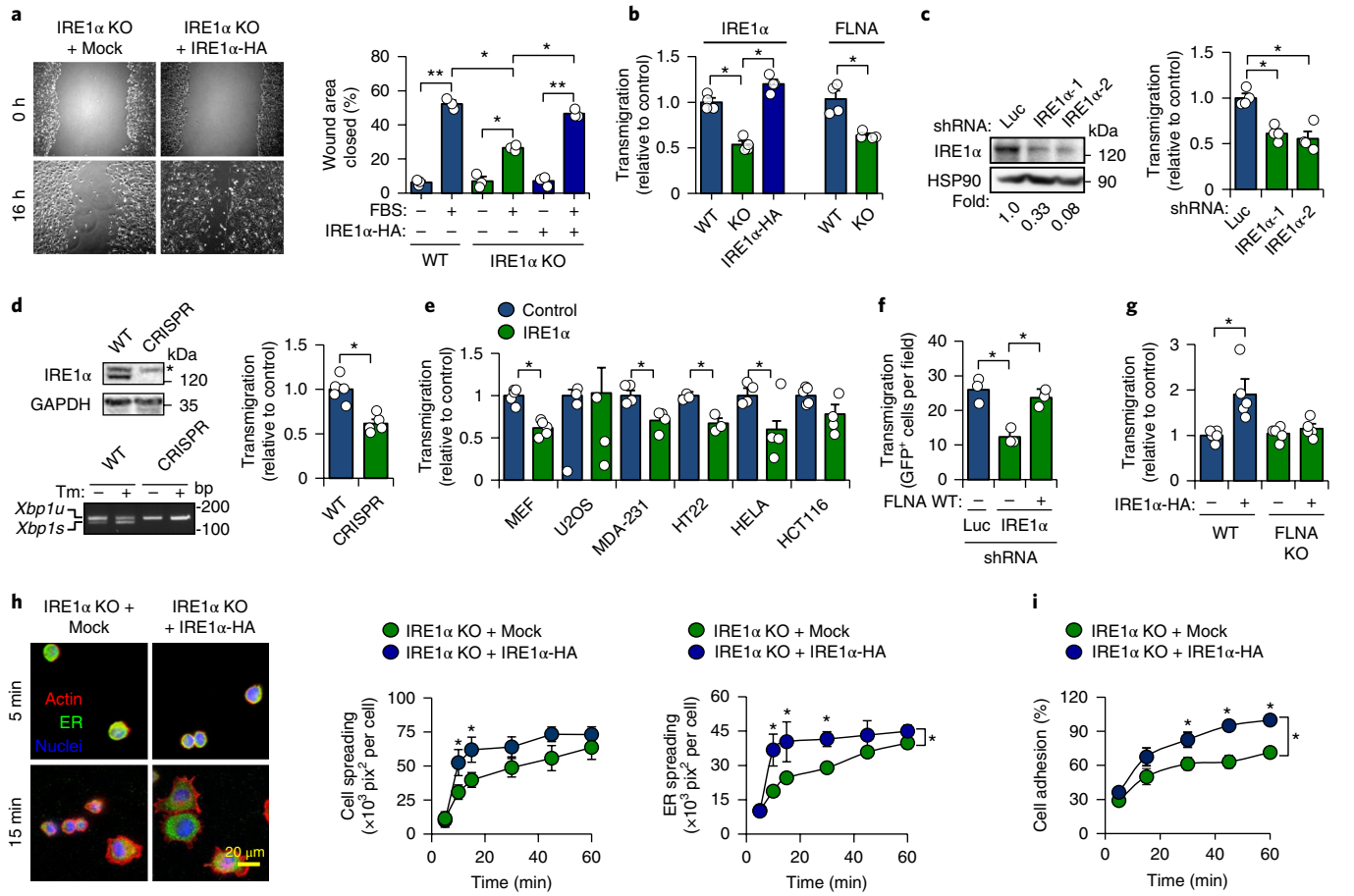

Fig. 3 | IRE1α expression enhances cell migration upstream of filamin A. a, Wound-healing assay results of confluent monolayers of WT, IRE1α KO and IRE1α-HA-reconstituted cells stimulated with 3% FBS and recorded at 0 and 16 h post-wounding (left) and quantified (right) ($n=5$ independent experiments). **b**, Transmigration of cells described in **a**, in addition to filamin A WT and KO MEFs using the Boyden chamber assay. After 4 h, cells were stained and counted ($n=4$ independent experiments). **c**, Knockdown was confirmed by western blotting in MEFs stably expressing two independent IRE1α shRNAs constructs or control (Luc). The percentage of IRE1α silencing is indicated. Right, Boyden chamber assay was performed in these cells using fibronectin-coated plates ($n=3$ independent experiments). **d**, Left, IRE1α KO MEF cells were generated using CRISPR–Cas9, followed by confirmation using western blotting (asterisk indicates nonspecific band) and *Xbp1* mRNA splicing assays (PCR fragments corresponding to the *Xbp1u* or *Xbp1s* forms are indicated). Right, Boyden chamber assay of control and IRE1α CRISPR KO cells (two-tailed *t*-test, $n=3$ independent experiments). **e**, Boyden chamber assay of indicated cell lines transfected with siRNA against IRE1α or a control siRNA for 48 h (two-tailed *t*-test, $n=4$). **f**, Boyden chamber assay of MEFs expressing control or IRE1α shRNA transiently transfected with a Myc-tagged filamin A vector or an empty vector followed by quantification of the number of GFP-positive cells in the lower chamber ($n=3$ independent experiments). **g**, Boyden chamber assay of FLNA WT and KO transiently transfected with pEGFP together with an expression vector for IRE1α-HA followed by quantification of number of GFP-positive cells in the lower chamber ($n=4$ independent experiments). **h**, Indirect immunofluorescence of IRE1α KO and IRE1α-HA-reconstituted cells stained with anti-KDEL antibody and phalloidin at different time points after seeding. Actin and ER total area was quantified as a measure of spreading ($n=3$ independent experiments, 50 cells in total). **i**, Cell adhesion assay in fibronectin-coated plates. Cells were stained with crystal violet and the total absorbance was measured ($n=3$ independent experiments). In all panels, data are shown as the mean ± s.e.m of the indicated number of independent experiments; one-way ANOVA followed by Tukey's test. $^*P<0.05$ and $^{**}P<0.01$.

rendered cells less sensitive to the inhibition of migration by the PKCα inhibitor Gö6976 (Fig. 5j). In agreement with this result, PKCα activation was decreased in IRE1α-deficient cells upon FBS stimulation (Supplementary Fig. 5J,K). We also detected an interaction between IRE1α, filamin A and PKCα in immunoprecipitation experiments (Fig. 5k). Using cellular fractionation and colocalization experiments, we observed a relocalization of PKCα to the ER in an IRE1α-dependent manner (Fig. 5l,m; see controls in Supplementary Fig. 5L). Taken together, these data indicate that IRE1α facilitates filamin A phosphorylation, which is mediated by PKCα, to induce actin cytoskeleton remodelling and cell migration.

IRE1α acts as a scaffold to regulate cell migration and filamin A phosphorylation. Since IRE1α is required for cell migration, we explored the contribution of XBP1 to this biological function. Remarkably, XBP1 deficiency or inhibition of the RNase activity of IRE1α had no impact on cell migration (Fig. 6a; Supplementary Fig. 6A). We also expressed IRE1α carrying different mutations that impair its kinase activity (K599A), kinase and endoribonuclease activity (P830L) or its ability to dimerize (D123P)[26]. Although all three IRE1α mutants lost their ability to catalyse *Xbp1* mRNA splicing under ER stress (Fig. 6b; Supplementary Fig. 6B), only the D123P variant impaired the pro-migratory activity of IRE1α (Fig. 6c; Supplementary Fig. 6C). Consistent with these results, the expression of the D123P mutant did not restore actin dynamics in IRE1α-null cells (Fig. 6d; Supplementary Fig. 6D). These findings indicate that IRE1α facilitates cell migration independent of its canonical signalling but requires its dimerization.

We studied IRE1α oligomerization using an IRE1α-GFP construct (IRE1-3F6H-GFP) to visualize IRE1α clustering[27].

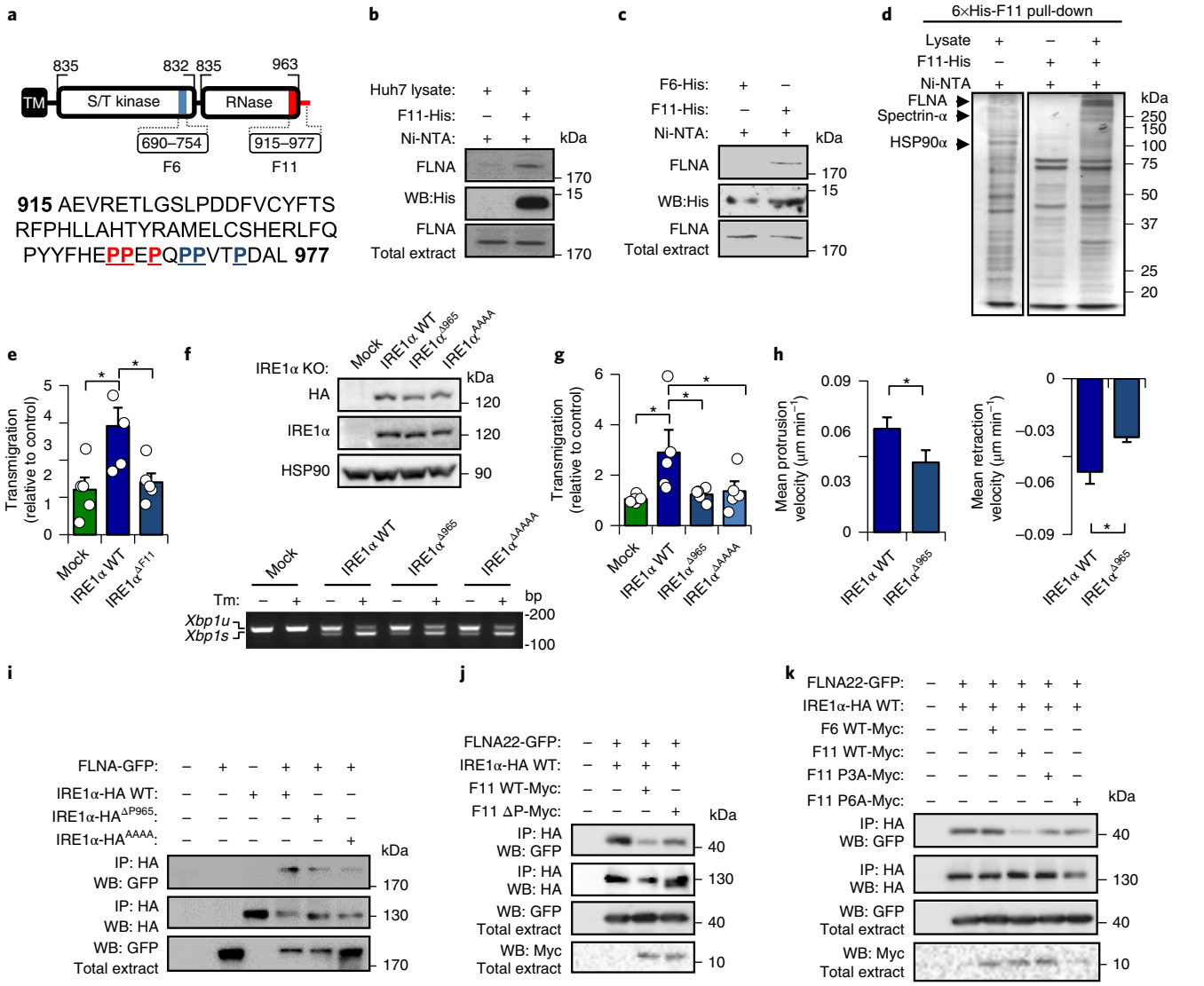

Fig. 4 | A physical interaction between IRE1α and filamin A is required for cell migration. a, Schematic representation of the C terminus of IRE1α divided into different fragments. The domains serine/threonin protein kinase (S/T kinase) and endoribonuclease (RNAse) are shown. A putative SH3-binding domain (PPXP) is shown in red and all prolines are highlighted in blue. **b**, Pull down of purified 6×HIS-F11 using Huh7 cell extracts and Ni-NTA (nickel-nitrilotriacetic acid) columns followed by western blotting. **c**, Pull down of purified 6×HIS-F11 or F6. **d**, Pull down of 6×HIS-F11 analysed by SDS–PAGE and Coomassie staining. Bands were analysed by mass spectrometry to identify the proteins. Images from the same gel were spliced together as indicated (see unprocessed gel scans). **e**, Boyden chamber assay of MEFs transfected with IRE1α WT or a deletion mutant of the F11 domain (ΔF11) ($n = 5$ independent experiments). **f**, Top, western blot of IRE1α knockout MEFs stably expressing IRE1α-HA WT, a deletion from amino acid P975 (Δ965), or a point mutant replacing PPEP for AAAA. Bottom, *Xbp1* mRNA splicing assay (RT-PCR) of indicated cells were treated with 100 ng ml^{-1} of Tm for 8 h. PCR fragments corresponding to the *Xbp1u* or *Xbp1s* forms are indicated. **g**, Boyden chamber assay of cells described in **f** seeded on fibronectin-coated transwell plates ($n = 5$ independent experiments). **h**, IRE1α KO cells reconstituted with WT or IRE1α Δ965 mutant were transfected with LifeAct and time-lapse confocal microscopy recordings were made. Protrusion and retraction velocity were determined using ADAPT software (two-tailed *t*-test; WT, $n = 20$ and IRE1α$^{\Delta 965}$ $n = 14$ independent experiments). **i**, Co-immunoprecipitation of IRE1α-HA (WT, Δ965 and AAAA mutants) and GFP-tagged filamin A was assessed by western blotting using HEK293T cells. **j**, Co-immunoprecipitation of IRE1α-HA and GFP-tagged-filamin A-22 domain in cells expressing F11 WT or a deleted peptide in the proline-rich sequence (F11ΔP) using HEK293T cells. **k**, Similar experiments were performed as in **j** using F11 WT or F11 P3A (proline substitution by alanine in three proline residues), F11 P6A (proline substitution by alanine in all six proline residues) or control F6 peptide. In all panels, data are shown as the mean ± s.e.m. of the indicated number of independent experiments; one-way ANOVA followed by Tukey's test was used unless otherwise indicated. *$P < 0.05$. Blots represent one out of two (**d**,**i**), or three (**b**,**c**,**j**,**k**) experiments, with similar results obtained.

IRE1-3F6H-GFP cells were tested in transmigration assays to monitor cells in the upper chamber (non-migrating) and cells in the lower chamber (migrating). An analysis of *Z*-stacks of cells in the lower chamber showed the presence of IRE1α-GFP clusters in ~22% of migrating cells (Fig. 6e). As a control, a D123P mutant was used in the same experiment to confirm that the signal was due to IRE1α oligomerization.

We then tested whether IRE1α dimerization is needed to interact and regulate filamin A. Immunoprecipitation experiments using the K599A, P830L and D123P mutants showed similar

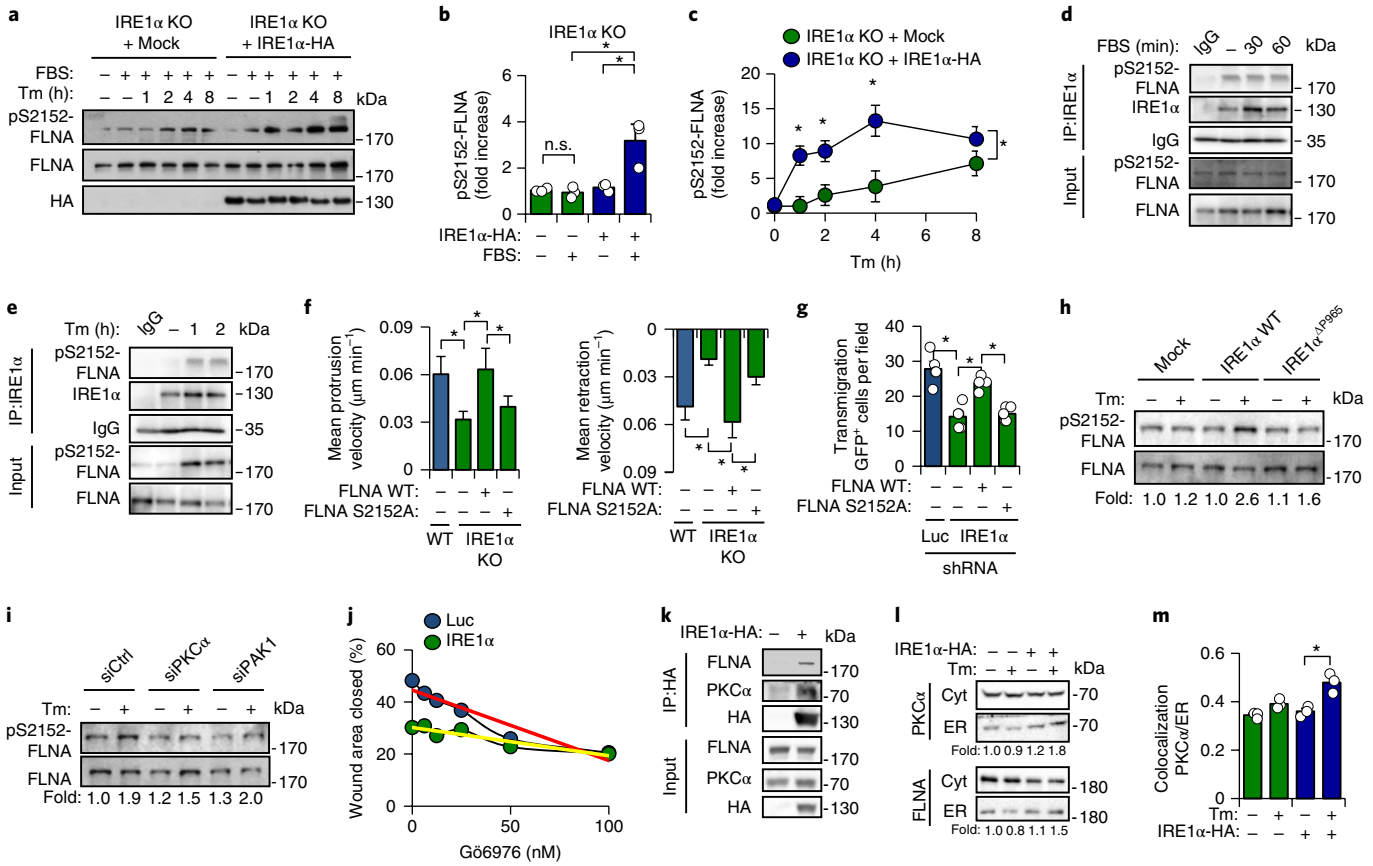

Fig. 5 | IRE1α regulates filamin A phosphorylation. a–c, Filamin A phosphorylation at S2152 was measured by western blotting in IRE1α KO and IRE1α-HA-reconstituted MEFs treated with FBS or Tm (**a**) followed by quantification (**b**,**c**) ($n=3$ independent experiments). **d**,**e**, Co-immunoprecipitation of endogenous IRE1α and filamin A in cells treated with 3% FBS (**d**) for 30-60 min or Tm (**e**) for 1–2 h. **f**, WT and IRE1α KO cells transfected with LifeAct and filamin A WT (FLNA-WT) or S2152A mutant filamin A (FLNA S2152A) were recorded by time-lapse confocal microscopy every 30 s for 5 min. Protrusion and retraction velocity was determined using ADAPT software (WT, $n=20$; KO $n=11$; KO + filamin A, $n=12$; KO + filamin A S2152A, $n=14$). **g**, Boyden chamber assay of shLuc or shIRE1α MEFs transiently transfected with pEGFP and expression vectors for FLNA-Myc or FLNA S2152A-Myc. Transmigration was evaluated by quantifying the number of GFP-positive cells in the lower chamber ($n=4$ independent experiments). **h**, Western blot of total protein extracts of IRE1α KO MEFs reconstituted with IRE1α-HA WT or IRE1α$^{\Delta P965}$ mutant treated with Tm for 2 h. **i**, Western blot of MEFs transfected with siRNAs against PKCα (siPKCα) and PAK1 (siPAK1) for 48 h followed by Tm treatment. **j**, Wound-healing assay of MEFs transfected with shRNA against Luc or IRE1α and treated with different concentrations of Gö6976 for 8 h. Slopes are indicated in red and yellow ($n=2$ independent experiments). **k**, Co-immunoprecipitation of IRE1α-HA with endogenous PKCα and filamin A. **l**, Subcellular fractionation was performed on IRE1α-deficient or reconstituted cells treated with Tm for 2 h. Pure microsomal (ER) and cytosolic (Cyt) fractions were analysed by western blotting. **m**, Colocalization of PKCα-FLAG and KDEL-RFP in transfected cells treated with Tm for 2 h (two-tailed *t*-test, $n=3$, 20 cells in total). In all panels, data represent the mean ± s.e.m. of the indicated number of independent experiments; one-way ANOVA followed by Tukey's test. $^*P<0.05$. n.s. not significant. Blots represent one out of two (**i**,**k**), or three (**d**,**h**,**i**,**l**) experiments, with similar results obtained.

associations with filamin A compared with wild-type IRE1α (Fig. 6f). However, interaction studies using the D123P mutant with the filamin A-22 domain alone indicated reduced binding under resting and ER stress conditions (Fig. 6g,h). Similar results were observed when IRE1α$^{\Delta 965}$ and IRE1α^{AAAA} mutants were tested (Fig. 6g). In addition, IRE1α expression favours the formation of dimers and larger order oligomers of filamin A (Fig. 6i). Remarkably, filamin A phosphorylation was abolished in IRE1α knockout cells expressing the D123P dimerization mutant (Fig. 6j). Taken together, these results suggest that IRE1α acts as a scaffold to recruit filamin A at resting conditions, inducing its phosphorylation upon IRE1α dimerization.

IRE1α regulates actin dynamics and cell migration in multiple model systems. To explore the physiological relevance of our findings, we used two in vivo models of cell migration coupled with genetic manipulation. We studied *Drosophila melanogaster* plasmatocytes (haemocytes), which are motile cells with functions and features similar to that of vertebrate macrophages[28]. Knocking down fly IRE1α (Ire1) by RNA interference resulted in reduced distance and velocity of movement (Fig. 7a; Supplementary Movie 2). Under these conditions, haemocytes exhibited an elongated morphology with reduced lamellipodia (Fig. 7b). Remarkably, overexpression of Cheerio (the filamin A form in *D. melanogaster*) fully rescued the migratory impairment triggered by knocking down fly IRE1α (Fig. 7a). To further examine the role of IRE1α in cell migration, we used an insertional Ire1 mutant coupled with a mosaic analysis, whereby only IRE1α-deficient cells are labelled with GFP[29] (scheme shown in Supplementary Fig. 7A). Primary cultures from Ire1α mutant cells were smaller in size area and showed reduced number of lamellar extensions (Fig. 7c). Remarkably, knocking down IRE1α led to a reduction of the retrograde flow of actin, reflected in a lower frequency in the velocity maps using the LifeAct reporter (Fig. 7d; Supplementary Movie 3). Taken together, these

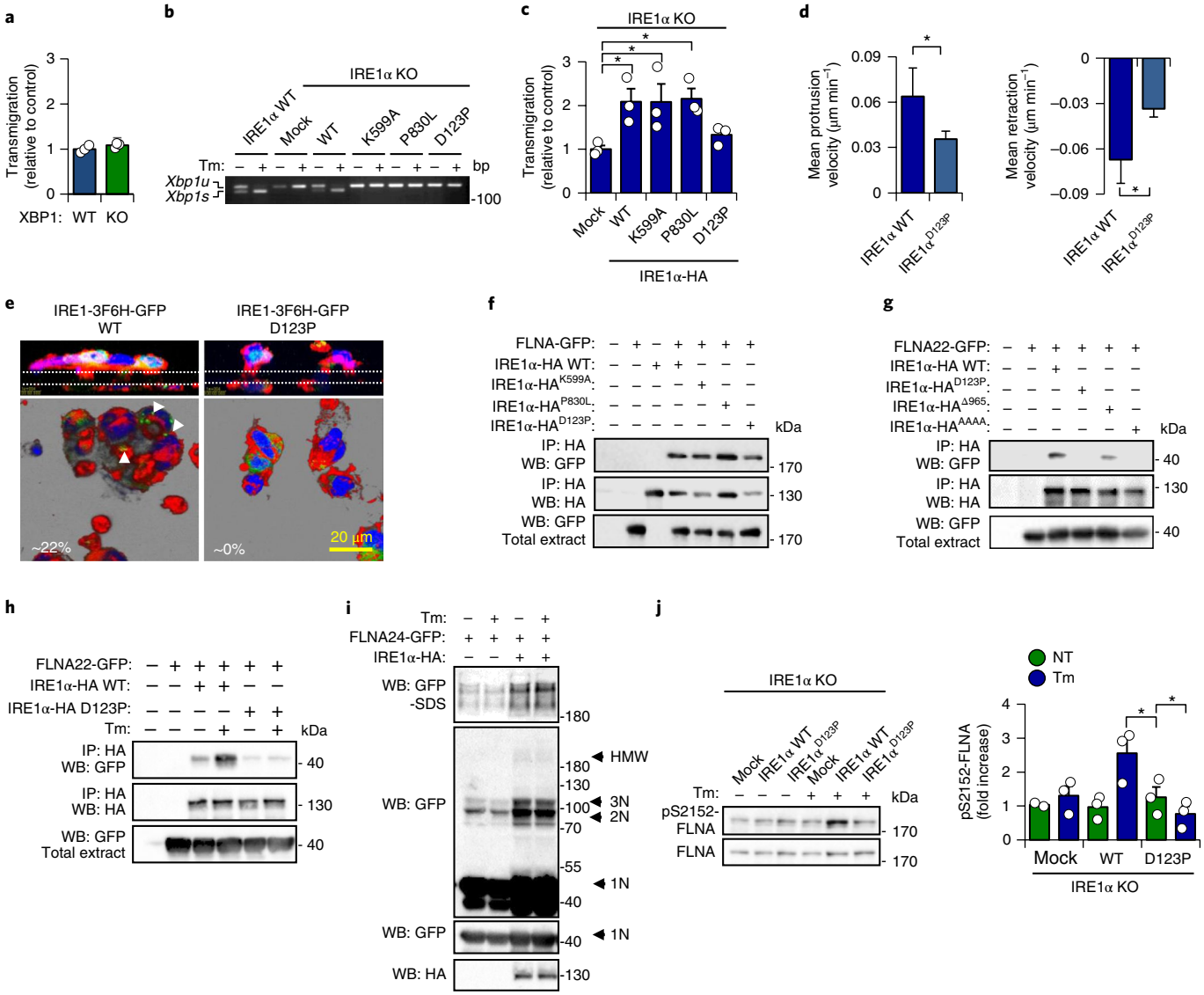

Fig. 6 | IRE1α dimerization, but not its enzymatic activities, controls cell migration and filamin A phosphorylation. a, Boyden chamber assay of XBP1-deficient or control MEFs. Transmigration was evaluated as described previously (two-tailed *t*-test, $n=3$) **b**, *Xbp1* mRNA splicing assay of indicated cells treated with Tm (K599A: kinase dead; P830L: kinase and RNase dead; D123P: non-dimerizing). **c**, Boyden chamber assay of IRE1α KO cells stably expressing IRE1α-HA WT, K599A, P830L or D123P mutants ($n=3$ independent experiments). **d**, Retractions and protrusions of IRE1α KO MEFs reconstituted with IRE1α WT or D123P mutant transfected with LifeAct were recorded by time-lapse confocal microscopy. The protrusion and retraction velocity were determined using ADAPT software (two-tailed *t*-test, IRE1α WT $n=20$, IRE1α^{D123P} $n=15$ independent experiments) **e**, Top, *Z*-stacks of TREX cells expressing IRE1-3F6H-GFP WT or IRE1-3F6H-GFP D123P mutant plated on transwell plates for 6 h and stained with phalloidin coupled to rhodamine. Lower panel: maximal projection of Z-stacks of cells in the lower chamber of a transwell. Arrowheads indicate IRE1α-GFP-positive foci. **f**, Co-immunoprecipitation of IRE1α-HA (WT, K599A, P830L and D123P) and GFP-tagged filamin A in HEK293T cells was assessed by western blotting. **g**, Co-immunoprecipitation of IRE1α-HA (WT, D123P, Δ965 and AAAA) and GFP-tagged filamin A-22 domain in HEK293T cells was analysed by western blotting. **h**, Co-immunoprecipitation of HA-tagged IRE1α (WT and D123P) and GFP-tagged filamin A-22 domain treated with Tm for 2 h was analysed by western blotting. **i**, Native-PAGE and western blot of HEK293T cells transfected with HA-tagged IRE1α and GFP-tagged filamin A-24 dimerization domain treated with Tm for 2 h. GFP-tagged filamin A-24 domain monomer (1N), dimer (2N), trimer (3N) and high molecular weight species (HMW) are indicated. **j**, Left, filamin A phosphorylation was assessed by western blotting of protein extracts from IRE1α KO cells expressing IRE1α-HA (WT, D123P or Mock) treated or not treated (NT) with with Tm. Right, quantification of the levels of filamin A phosphorylation in cells stimulated with FBS ($n=3$ independent experiments). In all panels, data represent the mean ± s.e.m. of the indicated number of independent experiments; one-way ANOVA followed by Tukey's test was used unless otherwise indicated. *$P<0.05$. Blots represent one out of two (**g**,**h**), or three (**f**,**i**,**j**) experiments, with similar results obtained.

results demonstrate a functional role of the IRE1α–filamin A axis in cell migration and actin dynamics in vivo in an invertebrate model.

We then assessed cell migration in zebrafish embryos, which show a well-characterized pattern of morphogenetic cell movements that are dependent on the actin cytoskeleton during gastrulation[30]. Three major stereotyped cell movements have been described: epiboly, convergence and extension (scheme shown in Fig. 7e). We blocked the activity of IRE1α during zebrafish development using a dominant-negative form (IRE1α-DN)[31,32] (Supplementary Fig. 7B) that also reduced filamin A phosphorylation in vitro

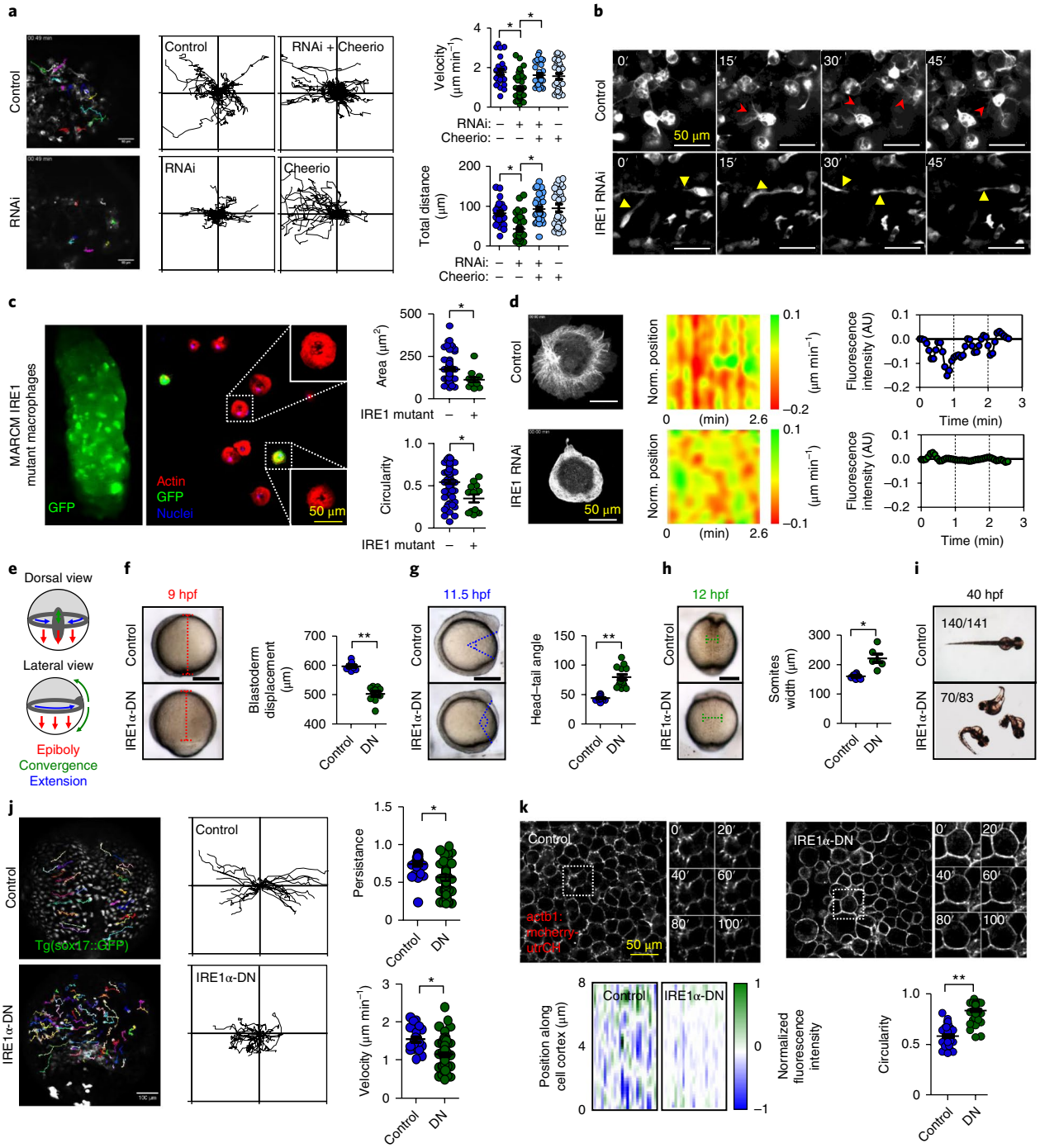

Fig. 7 | The activity of IRE1α in cell migration and actin dynamics is evolutionarily conserved. a, Cell movement trajectories of *D. melanogaster* macrophages expressing control or an IRE1α RNAi under the control of the HmlΔ-Gal4 driver. For rescue experiments, IRE1α RNAi and Cheerio P(EP) cheer^{G9093} were-co-expressed. Tracks were plotted (*x* and *y* axes correspond from -150 to 150 μm) (one-way ANOVA followed by Tukey's test; Control, $n=3$; IRE1α RNAi, $n=4$; and Cheerio, $n=3$ independent experiments). **b**, Time-lapse images of macrophages from **a**. Lamellipodia (red arrows) and filopodia (yellow arrows) are indicated. **c**, Images of macrophages from MARCM mutant animals (see Methods). GFP-positive cells (IRE1α mutant) or negative (control) were stained for F-actin (red) and DNA (blue) ($n=3$) **d**, Actin dynamics were recorded in time-lapse images of macrophages co-expressing LifeAct-GFP and IRE1α RNAi using the Cg-Gal4 driver (Control, $n=12$ and IRE1α RNAi, $n=9$). Velocity maps of representative cells for each condition were generated using the ADAPT tool. **e**, Schematic representation of the three morphogenetic movements during zebrafish gastrulation. **f**, Blastoderm displacement at 9 hpf was determined (broken red bracket). **g**, The angle formed between the radial lines that intersect the tip of the head and tail at 11.5 hpf was plotted. **h**, The width of the first three somites at 12 hpf was calculated (broken green bracket) (*n* for controls = 9 (**f**), 19 (**g**) or 8 (**h**); *n* for IRE1α-DN = 10 (**f**), 14 (**g**) or 6 (**h**)). **i**, Global phenotypes of embryos at 40 hpf are presented and quantified. **j**, Cell movement trajectories are shown of control and IRE1α-DN injected Tg(sox17::GFP) embryos at 7 hpf. The persistence and cell velocity of migrating cells was determined. **k**, Top, maximum projections of time-lapse confocal microscopy images of control and IRE1α-DN-injected Tg(actb1:mcherry-utrCH) embryos at 7 hpf. Time lapse images of higher magnification area is indicated (white square). Bottom, heatmap of normalized fluorescence intensity along the cell cortex of individual cells and cell circularity ($n=47$ for control; $n=61$ for IRE1α-DN). In all panels, data represent the mean ± s.e.m. of the indicated number of independent experiments; two-tailed *t*-test was used unless otherwise indicated. $^*P<0.05$ and $^{**}P<0.01$. Scale bars, 50 μm (**a**,**j**); 250 μm (**f**–**h**).

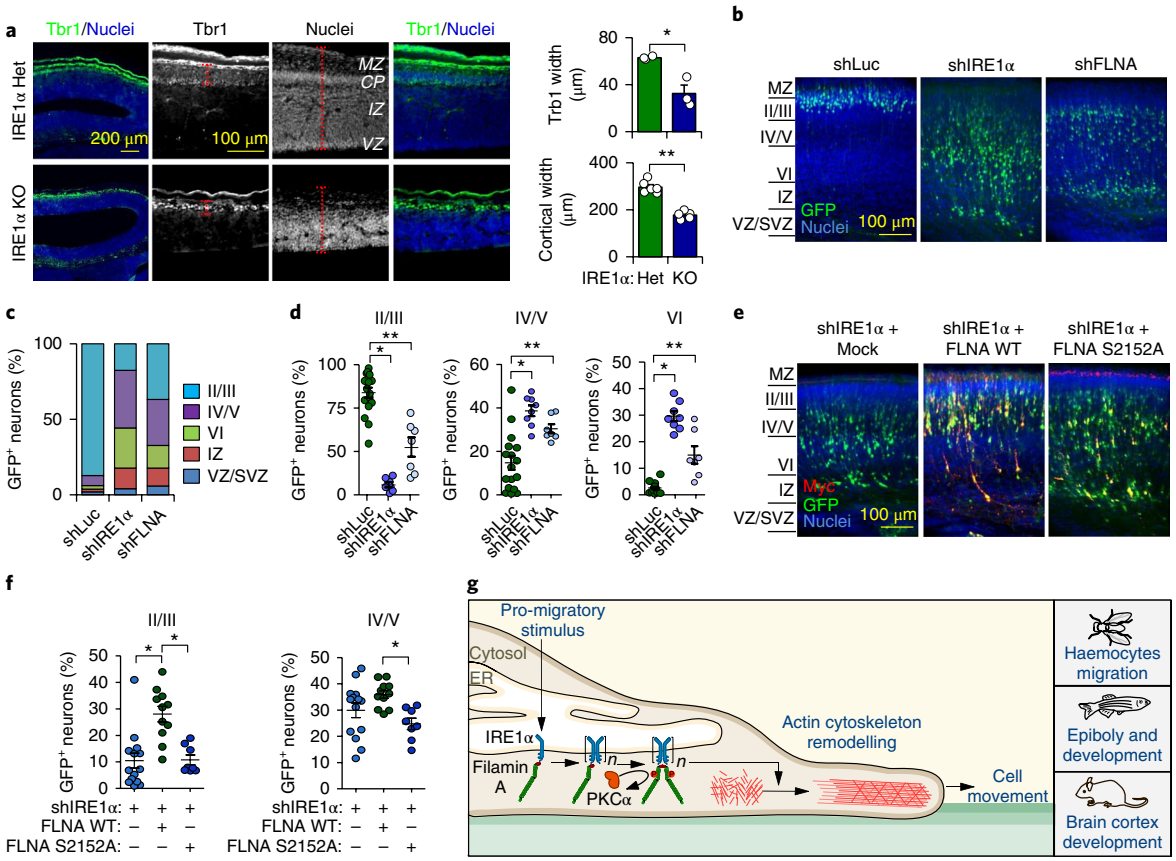

Fig. 8 | IRE1α is required for neuronal migration during brain cortex development. a, Left, IRE1α heterozygous (Het) or KO embryos were collected at E14.5 and brain tissue analysed by Trb1 and nuclei staining. MZ, marginal zone, CP, cortical plate; IZ, intermediate zone; VZ, ventricular zone. Global image is shown on the left, three magnified images are shown on the right. The dotted red lines indicate the area used for quantification. Right, quantification of Trb1 (two-tailed *t*-test, $n=3$) or cortical thickness (two-tailed *t*-test, $n=5$) (red dotted line). **b**, Coronal sections were visualized for transfected neurons (green) and cell nuclei using DAPI (blue). Merged images are shown. **c**, The percentage of GFP-positive cells was determined in different cortical brain layers for each mouse (shRNA Luc, $n=19$; shRNA IRE1α, $n=9$; and shRNA filamin A, $n=7$). VZ/subventricular zone (SVZ), IZ, layer VI (VI), layers IV/V (IV/V) and layers II/III (II/III) are shown. **d**, Individual dot plots of the analysis by cortical layer are shown for all groups. **e**, In utero co-electroporation was performed using shRNA to target IRE1α together with constructs expressing filamin A WT-Myc, filamin A S2152A-Myc or empty vector. Sections were stained for Myc using specific antibodies and visualized by fluorescence microscopy. **f**, The percentage of transfected GFP-positive cells was determined in indicated cortical layers in animals electroporated with shRNA IRE1α (Mock, $n=14$; filamin A WT-Myc, $n=11$; and filamin A S2152A-Myc, $n=7$). In all panels, the data are shown as the mean ± s.e.m. of the indicated number of independent experiments; one-way ANOVA followed by Tukey's test was used unless otherwise indicated. $^*P<0.05$ and $^{**}P<0.01$. **g**, Working model. The UPR transducer IRE1α signals through an unconventional mechanism that is independent of its enzymatic activities to control actin cytoskeleton dynamics. Monomeric IRE1α physically interacts with filamin A through a novel domain located at the distal C-terminal region. A pro-migratory stimulus triggers IRE1α dimerization, increasing the binding of filamin A and the recruitment of PKCα. Phosphorylation of filamin A at S2152 by PKCα increases actin cytoskeleton remodelling and cell migration in various animal species.

(Supplementary Fig. 7C). Remarkably, the vegetal progression of epiboly was delayed in IRE1α-DN embryos compared with control animals (Fig. 7f). Furthermore, this phenotype was associated with an increased head-to-tail angular separation (Fig. 7g) that is indicative of reduced anterior–posterior axial movements[33]. Finally, the width of the first somites at 12 h post fertilization was increased by ~40 % in IRE1α-DN embryos compared with controls (Fig. 7h), suggesting that the paraxial mesoderm suffered defective convergence. These alterations resulted in embryos with a shortened anterior–posterior axis at 24 h post fertilization (Fig. 7i), a phenotype that is suggestive of defective early gastrulation movements[34]. Importantly, none of these phenotypes were observed in embryos overexpressing wild-type IRE1α (Supplementary Fig. 7D).

We also observed reduced cell movement with single-cell tracking during the epiboly process (Fig. 7j; Supplementary Movie 4). In addition, using an actin reporter[35], we observed that epiblast cells of embryos injected with IRE1α-DN became rounded and less cohesive during gastrulation, showing reduced filopodial-like activity and increased formation of blebs compared with controls (Fig. 7k; Supplementary Movie 5). Moreover, the cortical distribution of F-actin appeared more homogeneous and less dynamic in IRE1α-DN embryos compared with controls (Fig. 7k; Supplementary Fig. 7E). Together, these experiments indicate that IRE1α expression has a fundamental and evolutionarily conserved activity in controlling actin cytoskeleton function and cell movement in vivo.

IRE1α deficiency alters radial migration of cortical neurons mimicking periventricular nodular heterotopia. Filamin A expression is essential for neuronal migration during brain cortex development, and mutations in the *FLNA* gene are the main cause of periventricular nodular heterotopia, a syndrome characterized by the abnormal localization of neurons along the walls of the lateral ventricle[36,37]. Full IRE1α deficiency is embryonic lethal, and the reported characterization did not include the study of brain

structures[38]. Therefore, we generated *IRE1α (Ern1)*-null animals and examined brain tissue at embryonic day 14.5 (E14.5). An analysis of post-mitotic cells of layer VI of the brain cortex after Tbr1 staining revealed a delay in the formation of this layer in IRE1α knockout animals compared with heterozygous mice (Fig. 8a). Similar observations were obtained when the width of the cortex was quantified (Fig. 8a).

We defined whether the morphological alterations observed during brain development in IRE1α-deficient animals were due to altered radial cell migration in vivo. We studied animals at E14.5 because high levels of filamin A and IRE1α were detected at that developmental stage (E12.5–14.5) (Supplementary Fig. 8C,D). We then performed in utero brain electroporation to knock down IRE1α in the developing cortex together with GFP at E14.5 to target cortical neural progenitors (strategy in Supplementary Fig. 8B). Normal development of neurons in layers II/III at birth was observed in control brains electroporated with a construct expressing a shRNA against luciferase mRNA (control). In contrast, brains electroporated with a shRNA to target IRE1α showed delayed migration (Fig. 8b). Quantification of neuronal distribution in cortical layers demonstrated that knocking down IRE1α resulted in a significant delay of neuronal migration, with cells accumulating at inferior cortical layers (Fig. 8c,d; Supplementary Fig. 8E). For comparison, we also knocked down filamin A, which also resulted in altered neuronal migration (Fig. 8b–d). Remarkably, electroporation of wild-type filamin A together with the shRNA targeting IRE1α, but not the filamin A S2152 mutant, rescued the detrimental effects of IRE1α deficiency in cortical neuronal migration, leading to a recovery in the percentage of cells reaching layer II/III and IV/V (Fig. 8e,f; Supplementary Fig. 8F,G). Overall, these results demonstrate that the regulation of filamin A by IRE1α plays an essential role in neuronal migration during brain cortex development.

Discussion

Although IRE1α represents the most conserved UPR signal transducer, its physiological function is still poorly understood. Most studies addressing the biological relevance of IRE1α in tissue homeostasis have been developed in artificial models of ER stress, and only a few reports support the existence of alternative activities of the pathway beyond protein-folding stress. Here, we identified filamin A as a major IRE1α interactor and uncovered a previously unanticipated function of this protein in the regulation of actin cytoskeleton dynamics, with a significant impact on cell migration in various model systems. Remarkably, although many interactome studies have been performed to identify novel IRE1α binding partners[2], no direct connections between IRE1α and cytoskeleton dynamics have been reported.

We characterized an unconventional signalling mechanism underlying IRE1α function, whereby it serves as a scaffold to recruit filamin A and potentiate the migratory capacity of the cell. We fully dissected the impact of IRE1α in cell migration, which is distinct from its classical role in the UPR and mediated by a previously uncharacterized proline-rich domain. We propose a two-step model whereby filamin A is associated to the ER through direct binding to IRE1α. Then, after stimulation with a pro-migratory stimulus, IRE1α dimerization and oligomerization induces a further recruitment of filamin A, scaffolding to PKCα, to increase filamin A dimerization and phosphorylation. This mechanism results in increased cytoskeleton dynamics (Fig. 8g). At the molecular level, we provide evidence to indicate that IRE1α increases filamin A phosphorylation at S2152, a specific regulatory event controlling cytoskeleton dynamics. One main question that remains to be addressed is the nature of the signals promoting IRE1α oligomerization during cell migration.

Alterations of filamin A are the underlying cause of periventricular nodular heterotopia, a human condition affecting brain development and is associated with mental retardation and cognitive impairment[36,37]. Our study demonstrates that targeting IRE1α phenocopies the consequences of filamin A deficiency in the developing brain. At least ten different regulators of filamin A are able to modulate neuronal migration[39], suggesting that a tight regulatory network that fine-tunes filamin A function is fundamental for brain development. Fingerprints of UPR activation were reported during the brain development in mouse, *Caenorhabditis elegans* and *D. melanogaster* models (reviewed previously[40]). Interestingly, PERK expression also affects brain development at the level of neurogenesis and the generation of intermediate progenitors and projection neurons of the brain cortex[41]. Moreover, the alternative activity of IRE1α described here may be relevant in the context of other diseases. FiIamin A has been proposed to contribute to the metastatic potential of cancer[42]. Thus, the IRE1α–filamin A axis may also enhance the occurrence of metastasis, an activity that may be insensitive to chemotherapy based on IRE1α RNase inhibitors. Overall, our study demonstrates a conserved function of IRE1α in actin cytoskeleton dynamics that is independent of its well-known role as an ER stress transducer, acting as a scaffold that recruits and potentiates filamin A function. Our findings illuminate how fundamental processes surveilling ER homeostasis are interconnected with the global machinery controlling cell movement.

Methods

Methods, including statements of data availability and any associated accession codes and references, are available at https://doi.org/10.1038/s41556-018-0141-0.

Received: 21 June 2017; Accepted: 13 June 2018;
Published online: 16 July 2018

References

1. Walter, P. & Ron, D. The unfolded protein response: from stress pathway to homeostatic regulation. *Science* **334**, 1081–1086 (2011).
2. Hetz, C., Chevet, E. & Oakes, S. A. Proteostasis control by the unfolded protein response. *Nat. Cell Biol.* **17**, 829–838 (2015).
3. Urra, H., Dufey, E., Lisbona, F. & Rojas-Rivera, D. When ER stress reaches a dead end. *Biochim. Biophys. Acta* **1833**, 3507–3517 (2013).
4. Oakes, S. A. & Papa, F. R. The role of endoplasmic reticulum stress in human pathology. *Annu. Rev. Pathol.* **10**, 173–194 (2015).
5. Wang, M. & Kaufman, R. J. Protein misfolding in the endoplasmic reticulum as a conduit to human disease. *Nature* **529**, 326–335 (2016).
6. Calfon, M. et al. IRE1 couples endoplasmic reticulum load to secretory capacity by processing the XBP-1 mRNA. *Nature* **415**, 92–96 (2002).
7. Lee, K. et al. IRE1-mediated unconventional mRNA splicing and S2P-mediated ATF6 cleavage merge to regulate XBP1 in signaling the unfolded protein response. *Genes Dev.* **16**, 452–466 (2002).
8. Hetz, C. & Glimcher, L. H. Fine-tuning of the unfolded protein response: Assembling the IRE1alpha interactome. *Mol. Cell* **35**, 551–561 (2009).
9. Feng, Y. & Walsh, C. A. The many faces of filamin: a versatile molecular scaffold for cell motility and signalling. *Nat. Cell Biol.* **6**, 1034–1038 (2004).
10. Oono, K. et al. JAB1 participates in unfolded protein responses by association and dissociation with IRE1. *Neurochem. Int.* **45**, 765–772 (2004).
11. Nakamura, F., Stossel, T. P. & Hartwig, J. H. The filamins: organizers of cell structure and function. *Cell Adhes. Migr.* **5**, 160–169 (2011).
12. Sepulveda, D. et al. Interactome screening identifies the ER luminal chaperone Hsp47 as a regulator of the unfolded protein response transducer IRE1alpha. *Mol. Cell* **69**, 238–252 (2018).
13. Nakamura, F., Osborn, T. M., Hartemink, C. A., Hartwig, J. H. & Stossel, T. P. Structural basis of filamin A functions. *J. Cell Biol.* **179**, 1011–1025 (2007).
14. Riedl, J. et al. Lifeact: a versatile marker to visualize F-actin. *Nat. Methods* **5**, 605–607 (2008).
15. Ridley, A. J. Rho GTPases and cell migration. *J. Cell Sci.* **114**, 2713–2722 (2001).
16. Vadlamudi, R. K. et al. Filamin is essential in actin cytoskeletal assembly mediated by p21-activated kinase 1. *Nat. Cell Biol.* **4**, 681–690 (2002).
17. Baldassarre, M. et al. Filamins regulate cell spreading and initiation of cell migration. *PLoS ONE* **4**, e7830 (2009).
18. Lynch, C. D. et al. Filamin depletion blocks endoplasmic spreading and destabilizes force-bearing adhesions. *Mol. Biol. Cell* **22**, 1263–1273 (2011).
19. van Vliet, A. R. et al. The ER stress sensor PERK coordinates ER-plasma membrane contact site formation through interaction with filamin-A and F-actin remodeling. *Mol. Cell* **65**, 885–899 (2017).

20. Ali, M. M. et al. Structure of the Ire1 autophosphorylation complex and implications for the unfolded protein response. *EMBO J.* **30**, 894–905 (2011).
21. Bouchecareilh, M., Higa, A., Fribourg, S., Moenner, M. & Chevet, E. Peptides derived from the bifunctional kinase/RNase enzyme IRE1α modulate IRE1α activity and protect cells from endoplasmic reticulum stress. *FASEB J.* **25**, 3115–3129 (2011).
22. Zhou, A.-X., Hartwig, J. H. & Akyürek, L. M. Filamins in cell signaling, transcription and organ development. *Trends Cell Biol.* **20**, 113–123 (2010).
23. Zhong, Z. et al. Cyclin D1/cyclin-dependent kinase 4 interacts with filamin A and affects the migration and invasion potential of breast cancer cells. *Cancer Res.* **70**, 2105–2114 (2010).
24. Tigges, U., Koch, B., Wissing, J., Jockusch, B. M. & Ziegler, W. H. The F-actin cross-linking and focal adhesion protein filamin A is a ligand and in vivo substrate for protein kinase C alpha. *J. Biol. Chem.* **278**, 23561–23569 (2003).
25. Sarkisian, M. R. et al. MEKK4 signaling regulates filamin expression and neuronal migration. *Neuron* **52**, 789–801 (2006).
26. Xue, Z. et al. A conserved structural determinant located at the interdomain region of mammalian inositol-requiring enzyme 1α. *J. Biol. Chem.* **286**, 30859–30866 (2011).
27. Li, H., Korennykh, A. V., Behrman, S. L. & Walter, P. Mammalian endoplasmic reticulum stress sensor IRE1 signals by dynamic clustering. *Proc. Natl Acad. Sci. USA* **107**, 16113–16118 (2010).
28. Wood, W. & Jacinto, A. Drosophila melanogaster embryonic haemocytes: masters of multitasking. *Nat. Rev. Mol. Cell Biol.* **8**, 542–551 (2007).
29. Lee, T. & Luo, L. Mosaic analysis with a repressible cell marker (MARCM) for Drosophila neural development. *Trends Neurosci.* **24**, 251–254 (2001).
30. Solnica-Krezel, L. & Sepich, D. S. Gastrulation: making and shaping germ layers. *Annu. Rev. Cell Dev. Biol.* **28**, 687–717 (2012).
31. Auf, G. et al. Inositol-requiring enzyme 1α is a key regulator of angiogenesis and invasion in malignant glioma. *Proc. Natl Acad. Sci. USA* **107**, 15553–15558 (2010).
32. Nguyen, D. T. et al. Nck-dependent activation of extracellular signal-regulated kinase-1 and regulation of cell survival during endoplasmic reticulum stress. *Mol. Biol. Cell* **15**, 4248–4260 (2004).
33. Hammerschmidt, M. et al. Mutations affecting morphogenesis during gastrulation and tail formation in the zebrafish, Danio rerio. *Development* **123**, 143–151 (1996).
34. Waxman, J. S., Hocking, A. M., Stoick, C. L. & Moon, R. T. Zebrafish Dapper1 and Dapper2 play distinct roles in Wnt-mediated developmental processes. *Development* **131**, 5909–5921 (2004).
35. Behrndt, M. et al. Forces driving epithelial spreading in zebrafish gastrulation. *Science* **338**, 257–260 (2012).
36. Fox, J. W. et al. Mutations in filamin 1 prevent migration of cerebral cortical neurons in human periventricular heterotopia. *Neuron* **21**, 1315–1325 (1998).
37. Sheen, V. L. et al. Mutations in the X-linked filamin 1 gene cause periventricular nodular heterotopia in males as well as in females. *Hum. Mol. Genet.* **10**, 1775–1783 (2001).
38. Iwawaki, T., Akai, R., Yamanaka, S. & Kohno, K. Function of IRE1 alpha in the placenta is essential for placental development and embryonic viability. *Proc. Natl Acad. Sci. USA* **106**, 16657–16662 (2009).
39. Sarkisian, M. R., Bartley, C. M. & Rakic, P. Trouble making the first move: interpreting arrested neuronal migration in the cerebral cortex. *Trends Neurosci.* **31**, 54–61 (2008).
40. Martinez, G., Khatiwada, S., Costa-Mattioli, M. & Hetz, C. ER proteostasis control of neuronal physiology and synaptic function. *Trends Neurosci.* https://doi.org/10.1016/j.tins.2018.05.009 (2018).
41. Laguesse, S. et al. A dynamic unfolded protein response contributes to the control of cortical neurogenesis. *Dev. Cell* **35**, 553–567 (2015).
42. Savoy, R. M. & Ghosh, P. M. The dual role of filamin A in cancer: can't live with (too much of) it, can't live without it. *Endocr. Relat. Cancer* **20**, R341–R356 (2013).

Acknowledgements

We thank P. Walter for providing IRE1-3F6H-GFP cells and M. P. Sheetz for providing filamin A-deficient cells and expression vectors. In addition, we thank D. Calderwood and D. Iwamoto for providing IgG-like filamin A individual plasmids tagged with GFP or GST. We thank L. Leyton for providing phospho-specific anti-PKC antibodies. This work was funded by the following bodies: FONDECYT no. 3160461 (to H.U.), no. 1140549 and 1180993 (to C.H.), no. 1140325 (to C.G.-B.), no. 1150608 (to R.L.V.); no. 1150766 (to F.C.); no. 3160478 (to E.P.); no. 3150113 (to A.C-S.) and no. 1140522 (to Á.G.); Millennium Institute No. P09-015-F (to C.H., A.C. and M.L.C.); FONDAP 15150012 (to C.H., F.C., C.G.-B. and M.L.C.); FONDAP 15090007 (to Á.G.); ECOS-CONICYT 170032 (to C.H.); PIA-CONICYT ACT1401 (to Á.G.); NIH R01 Gm113188 (L.Q.) and CONICYT ACT1402 (to M.L.C.). We also thank the following organizations: the European Commission R&D MSCA-RISE #734749; The Michael J Fox Foundation for Parkinson's Research—Target Validation grant No 9277; FONDEF ID16I10223; FONDEF D11E1007; the US Office of Naval Research-Global (ONR-G) N62909-16-1-2003; the US Air Force Office of Scientific Research FA9550-16-1-0384; ALSRP Therapeutic Idea Award AL150111; Muscular Dystrophy Association 382453; and CONICYT-Brazil 441921/2016-7 (to C.H.). T.I. is supported by the Toray Science Foundation. J.C., C.M.L (no. 21160967) and D.R.H. are doctoral fellows supported by a CONICYT fellowship and by a CONICYT research grant.

Author contributions

H.U and C.H. designed the study. H.U., D.R.H., J.C., D.V.-C., A.C.-S., E.C., E.P., E.M., Y.M.H., C.M.L., S.A.-R., R.F., R.L.V., R.A., D.A.R. and C.A:R. participated in experimental designs, performed experiments and analysed the data. R.L.V., F.C., A.C., L.Q., E.C., T.I., M.L.C., Á.G. and C.G.-B. supervised the experiments and participated in the designs. H.U and C.H. wrote or contributed to writing the manuscript. All authors read and approved the final version of the manuscript.

Competing interests

The authors declare no competing interests.

Additional information

Supplementary information is available for this paper at https://doi.org/10.1038/s41556-018-0141-0.

Reprints and permissions information is available at www.nature.com/reprints.

Correspondence and requests for materials should be addressed to C.H.

Publisher's note: Springer Nature remains neutral with regard to jurisdictional claims in published maps and institutional affiliations.

Methods

Reagents. Tunicamycin was purchased from Calbiochem EMB Bioscience. Cell culture media, fetal calf serum and antibiotics were obtained from Life Technologies. Fluorescent probes and secondary antibodies coupled to fluorescent markers were purchased from Molecular Probes, Invitrogen. All other reagents used were from Sigma or of the highest grade available.

Cell culture and DNA constructs. All MEFs and HEK cells were maintained in Dulbecco's modified Eagle's medium (DMEM) supplemented with 5% FBS, non-essential amino acids and grown at 37 °C and 5% CO_2. IRE1α-deficient cells were produced as previously described[6]. Briefly, retroviral plasmids were transfected using Effectene (Qiagen) into HEK293GPG cells in order to prepare IRE1α-HA expressing retroviruses were generated, as previously described[43], in the pMSCV-Hygro vector, whereby the IRE1α contains two tandem HA sequences at the C-terminal domain and a precision enzyme site before the HA tag. pRK5-F6 or F11 plasmids were generated as previously described[21]. Constructs of pEGFP expressing filamin A were generated as previously described[18]. Wild-type filamin A or S2152A mutants in pcDNA3.1 plasmids were a gift from J. Blenis (Addgene plasmid # 8982 and # 8983) (Weill Cornell Medicine, New York, NY). Wild-type filamin A or S2152A mutants in pcDNA3.1 plasmids were subcloned into the pCAGIG vector for in utero electroporation experiments[44].

Yeast-two hybrid assays. The interaction between the IRE1αΔN protein and a library of adult mouse cDNA was performed using a Matchmaker Gold Yeast Two-Hybrid System (Clontech) according to the manufacturer's protocols. Briefly, AH109 yeast cells were transformed with plasmid pGADT7 (bait) encoding the cytoplasmic domain of IRE1α (IRE1αΔN). The Y187 yeast strain contains the plasmid pGBKT7 (prey) encoding for a Normalized Yeast Two-Hybrid cDNA Library derived from adult mouse brain. Both plasmids encode for four different reporters: HIS3, ADE2, MEL1 and LacZ. AH109 and Y187 were mated for 24 h at 30 °C in YPDA media (common media containing yeast extract, peptone, dextrose and adenine). Mated yeasts were plated in synthetic defined medium SD-Leu/-Trp (DDO), SD-Leu/-Trp/-His (TDO) or SD-Leu/-Trp/-His/-Ade (QDO) for 3–7 days at 30 °C. The positive interactions were re-tested by re-streaking on TDO and QDO media after 3–7 days at 30 °C. Media lacking amino acids were also supplemented with X-α-galactoside (40 μg ml^{-1}), which changes the colonies that exhibit a positive interaction blue in colour. A growth index was calculated by visual observation (0 to 3 score) of the size and blue colouration of the selected colonies in TDO and QDO media. We used the interaction between pGBKT7-p53 and pGADT7-T as a positive control (Clontech). Plasmids of yeast colonies that showed positive interactions were rescued and transformed into *Escherichia coli* and then purified. Purified clones were then sequenced, and bioinformatics analysis was performed to identify target sequences.

To validate the interaction between IRE1α and filamin A, AH109 yeast cells were co-transformed with plasmid pGADT7-IRE1αΔN and pGBKT7-filamin A. Eight microlitres of each suspension and three subsequent tenfold serial dilutions were individually spotted onto a medium SD-Leu/-Trp, SD-Leu/-Trp/-His and SD (-Leu/-Trp/-His/X-α-Gal) plates for selection. Cells were incubated at 30 °C for 2 days.

RNA isolation, RT-PCR and real-time PCR. PCR primers and methods for the *Xbp1* mRNA splicing assay have been previously described[45]. *Xbp1s* mRNA was monitored by semi-quantitative PCR using the following primers: 5′-AAGAACACGCTTGGGAATGG-3′ and 5′-CTGCACCTGCTGCGGAC-3′. For the analysis of transcription targets and mRNA decay, real-time PCR assays were performed as described previously[46] using the following primers: Erdj4: 5′-CCCCAGTGTCAAACTGTACCAG-3′ and 5′- AGCGTTTCCAATTTTCCATAAATT-3′; β-actin: 5′-TACCACCAT GTACCCAGGCA-3′ and 5′-CTCAGGAGGAGCAATGATCTTGAT-3′; Blos1: 5′-TCCCGCCTGCTCAAAGAAC-3′ and 5′-GAGGTGATCCACCAACGCTT-3′; and Rpl19: 5′-CTGATCAAGGATGGGCTGAT-3′ and 5′-GCCGCTATGTA CAGACACGA-3′.

For mRNA analysis of cortex samples, real-time PCR assays were performed using the following primers: Ire1α: 5′-CTCAGGATAATGGTAGCCATGTC-3′ and 5′-ACACCGACCACCGTATCTCA-3′, filamin A: 5′-TGGGATGCTAG TAAGCCTGTG-3′ and 5′-CTGGGGTAATCACCTGAGGAAT-3′ and β-actin: 5′-CTCAGGAGGAGCAATGATCTTGAT-3′ and 5′- TACCACCAT GTACCCAGGCA-3.

Immunoprecipitation assays. HEK cells were co-transfected with different DNA constructs. After 48 h, protein extracts were prepared in lysis buffer (0.5% NP-40, 150–350 mM NaCL, 150 mM KCl, 50 mM Tris pH 7.6, 5% glycerol, 50 mM NaF, 1 mM Na_3VO_4, 250 mM PMSF, and protease inhibitors). Immunoprecipitation assays were performed as previously described[45]. In brief, to immunoprecipitate HA-tagged IRE1α, protein extracts were incubated with anti-HA antibody–agarose complexes (Roche) for 4 h at 4 °C, and then washed 3 times with lysis buffer (1 ml) and then once in lysis buffer with 500 mM NaCl. Protein complexes were eluted by heating at 95 °C for 5 min in loading buffer.

IRE1α-deficient MEFs cells stably transduced with retroviral expression vectors for IRE1α-HA or empty vector were incubated in the presence or absence of tunicamycin (500 ng ml^{-1}). Cell lysates were prepared for immunoprecipitation as described above for HEK cells. As a control, to eliminate nonspecific background binding, experiments were performed in parallel in IRE1α knockout cells. Protein complexes were eluted by heating at 95 °C for 5 min in loading buffer. Huh7 cells grown to subconfluency were lysed using 0.5% NP-40, 30 mM Tris-HCl pH 7.5, 150 mM NaCl, and proteases and phosphatases inhibitors (Complete, Phostop; Lysis Buffer) for 20 min at 4 °C, and lysates were clarified by centrifugation at 13,200 r.p.m. for 15 min. Clarified lysates were precleared with Protein A Sepharose beads (or magnetic beads) for 30 min at 4 °C. Precleared lysates were then incubated overnight with 5 μl ml^{-1} of lysate of anti-IRE1α antibodies (Santa Cruz Biotechnologies) at 4 °C followed by incubation with Protein A for 30 min at 4 °C. Beads were collected by centrifugation (30 s, 13,200 r.p.m. (rotor FA-45-18-11)) and washed 5 times with Lysis Buffer. Beads were dried and resuspended in sample buffer 2×. Samples were heated for 5 min at 95 °C and resolved by SDS–PAGE 8% followed by western blot analysis.

Expression of recombinant proteins. Expression and purification of the CRIB domain of PAK1 or the FLNA-19–21 and FLNA-21–24 IgG repeats were performed as described previously[47]. BL21 (DE3) *E. coli* strains carrying pGEX-glutathione S-transferase (GST)-CRIB were grown overnight at 37 °C in Luria broth media containing ampicillin. Cultures were diluted 1:100 and grown in fresh medium at 37 °C to an optical density at 600 nm of 0.7. Next, IPTG (isopropyl β-D-1-thiogalactopyranoside) was added to a final concentration of 1 mM. The cultures were grown for an additional 2 h and then samples were collected and sonicated in lysis buffer A (50 mM Tris-HCl pH 8.0, 1% Triton X-100, 1 mM EDTA, 150 mM NaCl, 25 mM NaF, 0.5 mM PMSF and protease inhibitor complex (Roche)). Cleared lysates were affinity purified with glutathione-Sepharose beads (Amersham). Loaded beads were washed ten times with lysis buffer B (lysis buffer A with 300 mM NaCl) at 4 °C. GST fusion protein was quantified and visualized in SDS–polyacrylamide gels stained with Coomassie brilliant blue.

Pull-down assays. FLNA-19–21 and FLNA-21–24 GST filamin domains bound to Sepharose-glutathione resin were incubated with 4 μg of the cytoplasmic domain of GST-tagged IRE1α for 6 h at 4 °C on an end-to-end rotor. After incubation, the mixture was centrifuged at 2,000 r.p.m. for 4 min and the supernatant was discarded. The resin was washed with 400 μl of lysis buffer at 4 °C for 10 min and subsequently centrifuged. This process was repeated five times. The bound proteins were eluted by boiling in SDS sample buffer at 95 °C for 5 min and analysed by western blotting.

Western blot analysis. Cells were collected and homogenized in RIPA buffer (20 mM Tris pH 8.0, 150 mM NaCl, 0.1% SDS, 0.5% Triton X-100) containing a protease inhibitor cocktail (Roche) in presence of 50 mM NaF and 1 mM Na_3VO_4. Protein concentrations were determined in all experiments by micro-BCA assay (Pierce), and 20-40 μg of total protein was loaded onto 8–12 % SDS–PAGE minigels (Bio-Rad Laboratories) before transfer onto polyvinylidene fluoride membranes. Membranes were blocked using PBS, 0.1% Tween20 (PBST) containing 5% milk for 60 min at room temperature then probed overnight with primary antibodies. The following antibodies diluted in blocking solution were used: anti-HSP90 (1:5000); anti-HA (1:1000; Roche); anti-GFP (1:3000; Sigma); anti-filamin A (1:1000); anti-phospho S2152 filamin A (1:1000); and anti-IRE1α (1:1000; Cell Signaling Technology). Bound antibodies were detected with peroxidase-coupled secondary antibodies (incubated for 1 h at room temperature) and an ECL system.

ER fractionation. Subcellular fractionation was performed following a previously described protocol[48]. In brief, cells were washed and ground in a stainless-steel dounce dura-grind tissue grinder (Wheaton). Cellular integrity was evaluated every five strokes with trypan blue staining. Homogenate was centrifuged 2 times at 640×*g* to remove unbroken cells and nuclei. Supernatant was centrifuged twice at 9,000×*g* to pellet crude mitochondria. The supernatant was further spun at 20,000×*g* for 30 min to obtain a pellet of lysosomes and plasma membrane and a supernatant that, upon further 100,000×*g* centrifugation, gave a supernatant (cytosol) and a pellet (ER). Western blot analyses were used to validate each fraction with different antibodies.

Indirect immunofluorescence analysis. IRE1α-HA, PKCα-Flag and KDEL proteins were visualized by immunofluorescence. Cells were fixed for 30 min with 4% paraformaldehyde and permeabilized with 0.5% NP-40 in PBS containing 0.5% bovine serum albumin (BSA) for 10 min. After blocking for 1 h with 10% FBS in PBS containing 0.5% BSA, cells were incubated with anti-HA, anti-Flag or anti-KDEL antibodies overnight at 4 °C. Cells were washed three times in PBS containing 0.5% BSA, and incubated with Alexa-conjugated secondary antibodies (Molecular Probes) for 1 h at 37 °C. Nuclei were stained with Hoechst dye. Coverslips were mounted with Fluoromount G onto slides and visualized by confocal microscopy (Fluoview FV1000).

We used a sensitive method based on a confined displacement analysis algorithm to calculate colocalization coefficients between IRE1α-HA and filamin A-GFP[49].

The colocalization of images was performed as previously described[49]. Briefly, images obtained by confocal microscopy using a ×60 oil objective lens (NA: 1.35) were subjected to Huygens deconvolution software. Each channel used for filamin A-GFP, IRE1α-HA and KDEL RFP (or Flag) was then segmented using a series of filters using IDL software to obtain masked images of each channel. These masked images were used to determine Manders colocalization coefficients and to quantify true and random colocalization between channels. In addition, a specific mask was applied to evaluate colocalization in the ER region (KDEL-RFP) or total cellular area (filamin A-GFP).

Targeting IRE1α in MEFs. We generated stable MEFs with reduced levels of IRE1α using previously described methods[50] by targeting IRE1α mRNA with two different shRNAs using the lentiviral expression vector pLKO.1 and puromycin selection. As a control, a shRNA against the luciferase gene was used. Constructs were obtained from The Broad Institute. Targeting sequences used for mouse IRE1α were as follows: GGAATCCTCTACATGGGTAAA and GCTGAACTACTTGAGGAATTA. To generate lentiviruses, HEK cells were transfected using the calcium phosphate protocol with 1 μg of VSV-G vector, 1 μg of Δ8.9 vector and 1 μg of shRNA vector. After 48 h of transfection, the supernatant was collected and filtered through a 0.45 μm filter. MEF cells were transduced with a 1:1 dilution of viral supernatant containing 8 μg ml^{-1} of polybrene. After 24 h of infection, cells were washed and incubated with 2 μg ml^{-1} of puromycin until selection was obtained. The CRISPR line IRE1α^{CRISPR} was generated using the mouse IRE1α Double Nickase system (Santa Cruz Biotechnology) as indicated by the manufacturer.

Cell migration assays. Confluent monolayers of MEF cells were wounded with a 20–200 ml pipette tip. Cells were washed twice with PBS and DMEM with 3% FBS was added as stimuli. Images were acquired using a ×10 objective lens and an inverted microscope at 0 and 16 h of migration. The wounded area was calculated using ImageJ software as previously described[51]. Transwell assays were performed in Boyden chambers (Transwell Costar, 6.5 mm diameter, 8 μm pore size) according to the manufacturer's instructions. Briefly, the bottom of the inserts were coated with 2 μg ml^{-1} fibronectin. Cells (3×10^4) re-suspended in serum-free medium were plated onto the top of each chamber insert and serum-free medium was added to the bottom chamber. After 4–6 h, inserts were removed, washed and cells that migrated to the bottom portion of the inserts were stained with 0.1% crystal violet in 2% ethanol and counted using an inverted microscope. In addition, cell-bound dye was eluted with methanol, and the absorbance was measured at 600 nm. For cell adhesion experiments, cells were plated on fibronectin-coated coverslips for different times. Cells were fixed with 4% paraformaldehyde and stained with 0.1% crystal violet in 2% ethanol to evaluate cell adhesion or processed for immunofluorescence to evaluate cell and ER spreading.

In addition, MEFs were co-transfected with different plasmids and pEGFP. Cells were re-seeded onto the top of each chamber insert coated with 2 μg ml^{-1} fibronectin and allowed to migrate for 4–6 h. Then, inserts were removed, washed and the number of GFP-positive cells was counted in 8 different fields using a fluorescent inverted microscope and a ×20 objective lens.

Actin cytoskeleton dynamics. MEF cells were seeded onto fibronectin-coated 25-mm coverslips, transfected with EGFP-Lifeact using Lipofectamine 2000 Transfection Reagent and imaged in HBSS medium supplemented with HEPES using a confocal microscope (Zeiss LSM 710) with a ×63/1.4 NA oil-immersion objective lens at 37 °C. Images were acquired every 30 s for 5 min, and the number of lamellipodia per cell was determined manually, as previously described[52]. In addition, to perform a protrusion and retraction analysis, images were segmented using maximum threshold[53]. Then, subsequent images were merged assigning the first image as green and the second image as red. The total area of green (protrusions) and red (retractions) colour of merged images was obtained using ImageJ software. In addition, cells were fixed and stained with phalloidin coupled to rodamine and visualized by confocal microscopy. The number of lamellipodia per cell was determined manually as described previously[52].

Rac1 activation assays. Purified loaded beads containing the CRIB domain were incubated for 70 min at 4 °C with 1 mg of either MEF lysates using fishing buffer (50 mM Tris-HCl pH 7.5, 10% glycerol, 1% Triton X-100, 200 mM NaCl, 10 mM $MgCl_2$, 25 mM NaF and protease inhibitor complex). The beads were washed three times with washing buffer (50 mM Tris-HCl pH 7.5, 30 mM $MgCl_2$ and 40 mM NaCl) and then re-suspended in SDS–PAGE sample buffer. Bound Rac1-GTP was subjected to immunoblot analysis and quantified with respect to total Rac1 using ImageJ.

IRE1α oligomerization assay. TREX cells expressing IRE1-3F6H-GFP wild-type or D123P were obtained from Cornell University and were generated as previously described[27]. TREX cells plated and treated with doxycycline (500 ng ml^{-1}) for 48 h. Cells were treated with tunicamycin (1 μg ml^{-1}) of for different time points and fixed with 4% paraformaldehyde for 30 min. Nuclei were stained with Hoechst dye. Coverslips were mounted with Fluoromount G onto slides and visualized by confocal microscopy (Fluoview FV1000). The number and size of IRE1α clusters were quantified using segmentation and particle analysis in ImageJ software.

Brain analysis of IRE1α knockout animals. Female and male IRE1α heterozygous mice were mated to obtain IRE1α heterozygous and knockout embryos. Both IRE1α knockout and control embryos at E14.5 were surgically collected from the pregnant IRE1α heterozygous mice. Each tail tip was immediately cut off from the embryonic body and was used for genotyping as previously described[38]. Then, each embryonic body was rinsed in PBS and then fixed in 4% paraformaldehyde phosphate buffer solution on a reciprocal shaker (50 osc. per min) for 24 h at room temperature. After fixation, each embryonic body was cryoprotected in 30% sucrose PBS on a reciprocal shaker (50 osc. per min) for 24 h at room temperature. Brains were collected and coronal sections were obtained for histological analyses, using anti-Trb1-specific antibodies and nuclei staining with DAPI. Images were obtained using an epifluorescence inverted microscope at ×10 and ×20 magnification. The width of the cortex and layer IV (Trb1 staining) was measured using ImageJ software. The experimental protocol (#2017-51) was approved by the Animal Studies Committees at Kanazawa Medical University and was compliant with all relevant ethical regulations regarding animal research.

In utero electroporation. In utero electroporation was performed as described previously[54,55]. Uterine horns of timed-pregnant dams were exposed by midline laparotomy after anaesthetization with isoflurane inhalation. A 2-μl solution containing 4 μg of DNA plasmid (shRNAs for IRE1α or a luciferase control co-expressed with a GFP-encoding vector at a 1:5 ratio) mixed with 0.02% fast green dye were injected into the lateral ventricles of E14.5 brains and then introduced into ventricular zone cells by delivering five electric pulses at 45 V for 50 ms, with 950 ms intervals, through the uterine wall using a Gene Pulser Xcell (Bio-Rad). After electroporation of all embryos, the uterus was replaced within the abdomen, the cavity was filled with warm sterile saline, and the abdominal muscle and skin incisions were closed with silk sutures. Animals were left to recover in a warm clean cage. Pups were harvested 5 days later (P0), and the position of transfected neurons in coronal sections was analysed by fluorescence microscopy. Cortex layers were identified via the nuclei density among the analysed section. The number of GFP-positive cells and total fluorescence intensity by layer was quantified using ImageJ software in all brain sections. All experiments were performed in accordance with the appropriate institutional guidelines of the Faculty of Medicine of the University of Chile and compliant with all relevant ethical regulations regarding animal research.

***D. melanogaster* strains and in vivo imaging.** The following strains were obtained from the Bloomington Stock Center: Cg-Gal4; HmlΔ-Gal4, 2xEGFP; UAS-mCD8-GFP; Iref02170/TM6B; hsFLP; Tub-Gal4, UAS-GFP/CyO, Act-GFP; Tub-Gal80TS, FRT82B P{EP}cher^{G9093}. UAS-Ire1-IR (v39562) was obtained from the Vienna Drosophila Research Center. All crosses were made at 25 °C. Pupae at 20 ± 2 h after puparium formation were mounted as described previously[56]. The migration of GFP-labelled macrophages was recorded using a Carl Zeiss LSM710 microscope with a ×40 objective. Movies are *Z*-projections of 12 1-μm slices acquired every 60 s for 50 min. Cells trajectories were recorded using the ImageJ Manual Tracking plugin, and their speed calculated using the Chemotaxis Tool plugin. The LifeAct-GFP reporter was expressed in macrophages using the Cg-Gal4 driver (Cg-Gal4 > LifeAct-GFP). After 75 min of culture, movies were recorded every 4 s for ~3 min using a Carl Zeiss LSM710 with a ×63 objective. Individual macrophages were recorded in the plane in which the largest membrane extension was observed. Velocity maps were generated using the ADAPT tool for imageJ as indicated previously[57]. For mosaic analysis, the following lines were crossed and grown at 25 °C: hsFLP; Tub-Gal4, UAS-GFP/CyO, Act-GFP; Tub-Gal80TS, FRT82B and Iref02170, FRT82B/TM6B. Progeny were subjected to a heat-shock of 1 h at 37 °C at 48, 72 and 96 h. After egg laying[29] third-instar larvae containing GFP-expressing macrophages were selected, and macrophage primary cultures were made.

To prepare primary culture coverslips, four third-instar larvae were washed in PBS then rinsed in 70% ethanol and washed once in PBS. Larvae were placed on coverslips with 120 μl Schneider's Insect Medium (Sigma-Aldrich), and immediately, a small incision was made in the posterior section of the cuticle using dissecting forceps. The haemolymph was collected for 1 min. Macrophages were allowed to adhere for 1 h and 15 min at 25 °C in a humidity chamber. The coverslip was then transferred to a 12-well plate, medium was removed and washed with PBS. For F-actin staining, cells were fixed in 4% paraformaldehyde for 10 min, permeabilized with PBS-0.1% Triton for 10 min and incubated for 2 h at room temperature with Phalloidin-FITC (50 μM, Sigma) in PBS-BSA 1%. TO-PRO-3 (10 μM; Invitrogen) was added in the last 20 min of incubation. Finally, cells were washed three times with PBS for 15 min each and mounted on Vectashield (Vector Laboratories). Imaging of cells was conducted using a Zeiss LSM710 microscope with ×63 objective. The images were processed using the software PHOTOSHOP CS4. All experiments were performed in accordance with the appropriate institutional guidelines of the Faculty of Medicine of the University of Chile and compliant with all relevant ethical regulations regarding animal research.

Zebrafish studies. Wild-type TAB5 and Tg(actb1:mCherry-utrCH) fish lines were used. Embryos were raised in E3 medium, kept at 28 °C and staged according to age (hours post fertilization; hpf). Sixty picograms of capped IRE1α-DN mRNA synthesized using a T7 mMessage mMachine Kit (Ambion) from the pcDNA-IRE1α-DN-DN[31,32], was injected into one-cell stage embryos as previously described[58] . To calculate the extent of cell movements during gastrulation, embryos were imaged using a stereoscope and the progression of the blastoderm, the head-to-tail angle and width of the first three somites were measured as previously described using Fiji free software at 9, 11.5 and 12 hpf[59]. For confocal imaging, Tg(actb1:mCherry-utrCH) embryos were placed in custom-made chambers and imaged on a Volocity ViewVox spinning disc (Perkin Elmer) coupled to a Zeiss Axiovert 200 confocal microscope using a Pan-Apochromatic × 40/1.2W objective. Images were deconvolved using Huygens software (Scientific Volume Imaging). To measure circularity and pixel signal intensity, cells were segmented manually using Fiji free software. All experiments were performed in accordance with the appropriate institutional guidelines of the Faculty of Medicine of the University of Chile and compliant with all relevant ethical regulations regarding animal research.

Statistics and reproducibility. For all experiments in cell lines, at least three independent biological experiments were performed. For all colocalization and electron microscopy experiments, we performed three independent biological experiments; however, since analysis was performed in individual cells, data analysis of all cells analysed are indicated in the legends. Results were statistically compared using one-way analysis of variance (ANOVA) for unpaired groups followed by multiple comparison post-tests (Tukey's multiple comparison test). When pertinent, two-tailed Student's *t*-test was performed for unpaired or paired groups. In all plots, *P* values are show as indicated: $^{*}P<0.05$, $^{**}P<0.01$ and $^{***}P<0.001$ and were considered significant. All results are presented as the mean ± s.e.m. Analyses were performed using PRISM software.

Reporting Summary. Further information on experimental design is available in the Nature Research Reporting Summary linked to this article.

Data availability. All data supporting the findings of this study are available from the corresponding author on reasonable request.

References

43. Hetz, C. et al. Proapoptotic BAX and BAK modulate the unfolded protein response by a direct interaction with IRE1alpha. *Science* **312**, 572–576 (2006).
44. Matsuda, T. & Cepko, C. L. Electroporation and RNA interference in the rodent retina in vivo and in vitro. *Proc. Natl Acad. Sci. USA* **101**, 16–22 (2004).
45. Lisbona, F. et al. BAX inhibitor-1 is a negative regulator of the ER stress sensor IRE1alpha. *Mol. Cell* **33**, 679–691 (2009).
46. Rodriguez, D. A. et al. BH3-only proteins are part of a regulatory network that control the sustained signalling of the unfolded protein response sensor IRE1alpha. *EMBO J.* **31**, 2322–2335 (2012).
47. Henriquez, D. R., Bodaleo, F. J., Montenegro-Venegas, C. & Gonzalez-Billault, C. The light chain 1 subunit of the microtubule-associated protein 1B (MAP1B) is responsible for Tiam1 binding and Rac1 activation in neuronal cells. *PLoS ONE* **7**, e53123 (2012).
48. Wieckowski, M. R., Giorgi, C., Lebiedzinska, M., Duszynski, J. & Pinton, P. Isolation of mitochondria-associated membranes and mitochondria from animal tissues and cells. *Nat. Protoc.* **4**, 1582–1590 (2009).
49. Ramirez, O., Garcia, A., Rojas, R., Couve, A. & Hartel, S. Confined displacement algorithm determines true and random colocalization in fluorescence microscopy. *J. Microsc.* **239**, 173–183 (2010).
50. Hetz, C. et al. The proapoptotic BCL-2 family member BIM mediates motoneuron loss in a model of amyotrophic lateral sclerosis. *Cell Death Differ.* **14**, 1386–1389 (2007).
51. Urra, H. et al. Caveolin-1-enhanced motility and focal adhesion turnover require tyrosine-14 but not accumulation to the rear in metastatic cancer cells. *PLoS ONE* **7**, e33085 (2012).
52. Lim, K. B. et al. The Cdc42 effector IRSp53 generates filopodia by coupling membrane protrusion with actin dynamics. *J. Biol. Chem.* **283**, 20454–20472 (2008).
53. Grande-Garcia, A. et al. Caveolin-1 regulates cell polarization and directional migration through Src kinase and Rho GTPases. *J. Cell Biol.* **177**, 683–694 (2007).
54. Fuentes, P., Canovas, J., Berndt, F. A., Noctor, S. C. & Kukuljan, M. CoREST/LSD1 control the development of pyramidal cortical neurons. *Cereb. Cortex* **22**, 1431–1441 (2012).
55. LoTurco, J., Manent, J. B. Sidiqi, F. New and improved tools for in utero electroporation studies of developing cerebral cortex. *Cereb. Cortex* **19**, 20–25 (2009).
56. Moreira, C. G., Regan, J. C., Zaidman-Remy, A., Jacinto, A. & Prag, S. *Drosophila* hemocyte migration: an in vivo assay for directional cell migration. *Methods Mol. Biol.* **769**, 249–260 (2011).
57. Barry, D.J., Durkin, C.H., Abella, J.V. & Way, M. Open source software for quantification of cell migration, protrusions, and fluorescence intensities. *J. Cell Biol.* **209**, 163–180 (2015).
58. Barth, K. A. & Wilson, S. W. Expression of zebrafish nk2.2 is influenced by sonic hedgehog/vertebrate hedgehog-1 and demarcates a zone of neuronal differentiation in the embryonic forebrain. *Development* **121**, 1755–1768 (1995).
59. Yeh, C. -M. et al. Ptenb mediates gastrulation cell movements via Cdc42/AKT1 in zebrafish. *PLoS ONE* **6**, e18702 (2011).

nature research

Corresponding author(s): Claudio Hetz

Reporting Summary

Nature Research wishes to improve the reproducibility of the work that we publish. This form provides structure for consistency and transparency in reporting. For further information on Nature Research policies, see Authors & Referees and the Editorial Policy Checklist.

Statistical parameters

When statistical analyses are reported, confirm that the following items are present in the relevant location (e.g. figure legend, table legend, main text, or Methods section).

n/a	Confirmed
☐	☒ The exact sample size (*n*) for each experimental group/condition, given as a discrete number and unit of measurement
☒	☐ An indication of whether measurements were taken from distinct samples or whether the same sample was measured repeatedly
☐	☒ The statistical test(s) used AND whether they are one- or two-sided *Only common tests should be described solely by name; describe more complex techniques in the Methods section.*
☐	☒ A description of all covariates tested
☐	☒ A description of any assumptions or corrections, such as tests of normality and adjustment for multiple comparisons
☐	☒ A full description of the statistics including central tendency (e.g. means) or other basic estimates (e.g. regression coefficient) AND variation (e.g. standard deviation) or associated estimates of uncertainty (e.g. confidence intervals)
☒	☐ For null hypothesis testing, the test statistic (e.g. *F*, *t*, *r*) with confidence intervals, effect sizes, degrees of freedom and *P* value noted *Give P values as exact values whenever suitable.*
☒	☐ For Bayesian analysis, information on the choice of priors and Markov chain Monte Carlo settings
☒	☐ For hierarchical and complex designs, identification of the appropriate level for tests and full reporting of outcomes
☒	☐ Estimates of effect sizes (e.g. Cohen's *d*, Pearson's *r*), indicating how they were calculated
☐	☒ Clearly defined error bars *State explicitly what error bars represent (e.g. SD, SE, CI)*

Our web collection on statistics for biologists may be useful.

Software and code

Policy information about availability of computer code

Data collection	For co-localization a three step processes was done. First deconvolution of images were done using Huygens Professional software. Second, segmentation and total and endoplasmic reticulum (ER) masks were done using IDL 7.0. Finally, colocalization between IRE1a/ Filamin A, Filamin A/ER and PKCa/ER was done using Colocalization displacement analysis available in IDL7.0 or Image J software. All quantifications of number of cell of transmigration assays, area of wound in healing assays, total and ER area of adhesion assays and width measurement were done using Image J software. Gene Ontology analysis of proteins obtained in the Yeast-two hybrid screen was done using Toppgene analysis available online
Data analysis	Data acquisition and graphs were done in excel files and statistical analysis were done using GraphPad Prism 5 software.

For manuscripts utilizing custom algorithms or software that are central to the research but not yet described in published literature, software must be made available to editors/reviewers upon request. We strongly encourage code deposition in a community repository (e.g. GitHub). See the Nature Research guidelines for submitting code & software for further information.

Data

Policy information about availability of data

All manuscripts must include a data availability statement. This statement should provide the following information, where applicable:

- Accession codes, unique identifiers, or web links for publicly available datasets
- A list of figures that have associated raw data
- A description of any restrictions on data availability

All data and materials along with detailed instructions on their use are available from the authors upon request. No raw data have been linked in the manuscript.

Field-specific reporting

Please select the best fit for your research. If you are not sure, read the appropriate sections before making your selection.

☒ Life sciences ☐ Behavioural & social sciences ☐ Ecological, evolutionary & environmental sciences

For a reference copy of the document with all sections, see nature.com/authors/policies/ReportingSummary-flat.pdf

Life sciences study design

All studies must disclose on these points even when the disclosure is negative.

Sample size	All experiments performed in this work were repeated at least three times, unless indicated otherwise in individual figure legends. All repeats performed resulted in exact agreement or similar results. No sample size calculation were performed for in vitro experiments and sample sizes were chosen for individual experiments according to pur previous expertise. For cellular based-assays we repeat a minimun of 4 experiments in order to perform statistical analysis. For in vivo experiments using in utero electroporation we define a minimum of experimental animals based on the indications suggested in "Guidelines for the Care and Use of Mammals in Neuroscience and Behavioral Research" using the following model n=1+2C(s/d)^2 (n is the number of animals; C is a constant that depend on the power and statistical differences; s is the standard deviation of the measurement and d is the differences expected in each condition)
Data exclusions	No data was excluded from the analysis.
Replication	For immunoprecipitation experiments every time we prepared freshly made lysis buffer we stock solutions. For endogenous IP we always used a 10 cm plate containing around 7x106 cells. For IP using over expression of proteins we transfected 2 well of 6-well plates. Transfection efficiency was observed every time to be sure to have enough material. Although initial experiments were hard to observe the co-IP, once we setup the right buffer we always observed the co-IP of Filamin A and IRE1a. For cell culture experiments, we track the passage of cells in order to used cells in similar passages and used new batch after 10 passages. Selection of cells was done every two week to always work with cells expressing WT and mutant IRE1a. Wound healing assays, transmigration and actin cytoskeleton dynamics were done almost at same days or weeks to ensure reproducibility. Since working with tunicamycin is complicated since freezing cycles affects the stability of the molecule we always used small aliquots that only have been thawed once in order to ensure reproducibility.
Randomization	For in utero electroporation samples were devided in control and the experimental condition based in the position in the uterine horns. Left side of the uterine horns were injected with control conditions always. The experimental condition was injected in pups in the right side of the horns. No randomization was done
Blinding	Quantification of actin bundles by EM and the GFP% neurons in the in utero electroporation experiments were done blinded.

Reporting for specific materials, systems and methods

Materials & experimental systems

n/a	Involved in the study
☐	☒ Unique biological materials
☐	☒ Antibodies
☐	☒ Eukaryotic cell lines
☒	☐ Palaeontology
☐	☒ Animals and other organisms
☒	☐ Human research participants

Methods

n/a	Involved in the study
☒	☐ ChIP-seq
☒	☐ Flow cytometry
☒	☐ MRI-based neuroimaging

Unique biological materials

Policy information about availability of materials

Obtaining unique materials: All unique materials used are available

Antibodies

Antibodies used:

Antibody Anti-HA High Affinity 3F10
Supplier name: Roche
Catalog number 11867423001
Dilution 1:3000
Used as recommended by manufacturer
Antibody Anti-GFP (B-2)
Supplier name: Santa cruz biotechnology
Catalog number SC-9996
Dilution 1:3000
Used as recommended by manufacturer
Antibody Anti-Filamin A
Supplier name: Cell Signaling Technology
Catalog number 4762
Dilution 1:1000
Used as recommended by manufacturer
3
nature research | reporting summary March 2018
Antibody Anti-pS2152-Filamin A
Supplier name: Cell Signaling Technology
Catalog number 4761
Dilution 1:1000
Used as recommended by manufacturer
Antibody Anti-Filamin A
Supplier name: ABCAM
Catalog number ab76289
Dilution 1:5000
Used as recommended by manufacturer

Antibody Anti-pS2152-Filamin A
Supplier name: ABCAM
Catalog number ab51229
Dilution 1:1000
Used as recommended by manufacturer

Antibody Anti-Glutathione-S-Transferase (GST) antibody produced in rabbit
Supplier name: Santa cruz biotechnology
Catalog number sc-53909
Dilution 1:1000
Used as recommended by manufacturer

Antibody Anti-IRE1a
Supplier name: Cell Signaling Technology
Catalog number 3294S
Dilution 1:1000
Used as recommended by manufacturer

Antibody Anti-Rac1 Clone 102
Supplier name: BD Transduction Laboratories
Catalog number 610650
Dilution 1:5000
Used as recommended by manufacturer

Antibody Anti-HSP90
Supplier name: Santa cruz biotechnology
Catalog number SC-7947
Dilution 1:5000
Used as recommended by manufacturer

Antibody Anti-KDEL
Supplier name: Enzo Life Sciences
Catalog number SPA-827
Dilution 1:200 (IFI)
Used as recommended by manufacturer

Antibody Anti-HIS
Supplier name: Santa cruz biotechnology
Catalog number sc-803
Dilution 1:1000
Used as recommended by manufacturer

Antibody Anti-Trb1
Supplier name: Abcam
Catalog number ab31940
Dilution 1:200 (IFI)
Used as recommended by manufacturer

Antibody Anti-Myc
Supplier name: Santa cruz biotechnology
Catalog number sc-40
Dilution 1:1000
Used as recommended by manufacturer

Validation

For most of endogenous proteins tested we validated the antibody using the WT and Knockout proteins. For the antibodies used for IP, the antibody was tested using the over expression of tagged proteins.
All antibodies used for indirect inmmunofluorescence we performed primary and secondary antibodies control in addition to used en knockout cells.

Eukaryotic cell lines

Policy information about cell lines

Cell line source(s)

MEF IRE1 WT and knockout cells were provided David Ron. From this cell lines we reconstitute with IRE1a WT and the different mutants tested in the manuscript. All other cells used including HEK-293 (ATCC), MDA-231, HT22, HELA and HCT116 were obtained from the University of Chile. The cell line U2OS was obtained from Guido Kroemer laboratory.

Authentication

Since cell lines were obtained from animals in a previously described publication and their are not commercially available we did not performed any cell line authentication. We surely perform validation of knockout cells by PCR and western blot of selected proteins. To evaluate the activity of IRE1a mutants we performed XBP1 mRNA splicing assay as described in methods.

Mycoplasma contamination

All cells were negative for mycoplasma contamination. All cells were routinely tested for mycoplasma contamination using the EZ-PCR Mycoplasma Test Kit (Biological Industries). In case of any contamination, the cell line was eliminated inmediatly and a new batch was thawed.

Commonly misidentified lines
(See ICLAC register)

No common misidentified cell lines were used

Animals and other organisms

Policy information about studies involving animals; ARRIVE guidelines recommended for reporting animal research

Laboratory animals

For in utero electroporation experiments we used pregnant female mice and intervened at E14.5 and at P0.

For the embryo analysis of IRE1 Knockout animals we used Female and male IRE1α Heterozygous (Het) C57BL6 mice mated to obtain IRE1α Het and KO embryos. Both IRE1α KO and control embryos were surgically collected from the pregnant IRE1α Het mice at 14.5.

For D. Melanogaster experiments we used several strains obtained from Bloomington stock center: Cg-Gal4; HmlΔ-Gal4, 2xEGFP; UAS-mCD8-GFP; Iref02170/TM6B; hsFLP; Tub-Gal4, UAS-GFP/CyO, Act-GFP; Tub-Gal80TS. FRT82B P{EP}cherG9093 are from the Vienna Drosophila Research Center: UAS-Ire1-IR (v39562). For all experiments we used pupae at 20 ±2 h APF (After Puparium Formation)

For Zebrafish experiments we used several strains available in Miguel Concha's Laboratory including Wild-type TAB5, Tg(actb1:mCherry-utrCH) and Tg(sox17::GFP). Embryos were used at 1-cell stage embryos to inject mRNAs and then analyzed at

	7, 9, 11.5 and 12 hpf depending on the experiment.
Wild animals	The study did not involve wild animals, no animals in the study were collected from the field
Field-collected samples	The study did not involve wild animals, no animals in the study were collected from the field